ARTICLES
https://doi.org/10.1038/s41590-022-01222-1

nature immunology

Check for updates

Targeted isolation of diverse human protective broadly neutralizing antibodies against SARS-like viruses

Wan-ting He[1,2,3,11], Rami Musharrafieh[1,2,3,11], Ge Song[1,2,3,11], Katharina Dueker[1,2,3,11], Longping V. Tse[4], David R. Martinez[4], Alexandra Schäfer[4], Sean Callaghan[1,2,3], Peter Yong[1,2,3], Nathan Beutler[1], Jonathan L. Torres[5], Reid M. Volk[5], Panpan Zhou[1,2,3], Meng Yuan[5], Hejun Liu[5], Fabio Anzanello[1,2,3], Tazio Capozzola[1,2,3], Mara Parren[1], Elijah Garcia[1], Stephen A. Rawlings[6], Davey M. Smith[6], Ian A. Wilson[2,3,5,7], Yana Safonova[8], Andrew B. Ward[2,3,5], Thomas F. Rogers[1,6], Ralph S. Baric[4,9] ✉, Lisa E. Gralinski[4] ✉, Dennis R. Burton[1,2,3,10] ✉ and Raiees Andrabi[1,2,3] ✉

The emergence of current severe acute respiratory syndrome coronavirus 2 (SARS-CoV-2) variants of concern (VOCs) and potential future spillovers of SARS-like coronaviruses into humans pose a major threat to human health and the global economy. Development of broadly effective coronavirus vaccines that can mitigate these threats is needed. Here, we utilized a targeted donor selection strategy to isolate a large panel of human broadly neutralizing antibodies (bnAbs) to sarbecoviruses. Many of these bnAbs are remarkably effective in neutralizing a diversity of sarbecoviruses and against most SARS-CoV-2 VOCs, including the Omicron variant. Neutralization breadth is achieved by bnAb binding to epitopes on a relatively conserved face of the receptor-binding domain (RBD). Consistent with targeting of conserved sites, select RBD bnAbs exhibited protective efficacy against diverse SARS-like coronaviruses in a prophylaxis challenge model in vivo. These bnAbs provide new opportunities and choices for next-generation antibody prophylactic and therapeutic applications and provide a molecular basis for effective design of pan-sarbecovirus vaccines.

Relatively early in the coronavirus disease 2019 (COVID-19) pandemic, it appeared that SARS-CoV-2 was a virus that might be particularly amenable to control by vaccination. Many different vaccine modalities, most notably messenger RNA vaccination, showed spectacular success in phase 3 protection studies[1,2]. The success was attributed at least in part to the ability of the different modalities to induce robust nAb responses[3–5]. However, since the virus has now infected hundreds of millions worldwide, variants have arisen (VOCs), some of which show notable resistance to neutralization by immunodominant nAb responses induced through infection and vaccination[6–10]. Current vaccines are still apparently largely effective in preventing hospitalization and death caused by VOCs[11,12]. However, as vaccine-induced nAb responses naturally decline, breakthrough infections are on the increase and there are concerns that these may become more prevalent and perhaps more clinically serious, and that more pathogenic and resistant VOCs may appear. There are also concerns that emerging SARS-like viruses may seed new pandemics from spillover events[13,14].

These concerns drive a search for nAbs and vaccines that are effective against a greater diversity of sarbecoviruses. Indeed, several individual bnAbs have now been generated either by direct isolation of bnAbs from convalescent donors or from antibody engineering of more strain-specific nAbs to generate breadth[15–23]. Ideally, large panels of bnAbs would provide more options in the use of such Abs for prophylaxis and therapy[24]. Importantly, a range of bnAbs would allow for better definition of the requirements for neutralization breadth and more rational effective design of appropriate immunogens[25,26]. A range of bnAbs has been crucial in germline-targeting approaches to HIV vaccine design[25–29]. Inspired by the demonstration[18,30–40] of the strong serum nAb responses in individuals who are infected with SARS-CoV-2 and then receive an mRNA vaccine, we isolated and characterized 40 bnAbs from 2 donors convalescing from COVID-19 who were recently vaccinated, many of which combine excellent potency and breadth to sarbecoviruses. *In* vivo evaluation of select RBD bnAbs in a prophylaxis challenge model showed robust protection against diverse angiotensin-converting enzyme 2 (ACE2)-utilizing sarbecoviruses.

[1]Department of Immunology and Microbiology, The Scripps Research Institute, La Jolla, CA, USA. [2]International AIDS Vaccine Initiative Neutralizing Antibody Center, The Scripps Research Institute, La Jolla, CA, USA. [3]Consortium for HIV/AIDS Vaccine Development, The Scripps Research Institute, La Jolla, CA, USA. [4]Department of Epidemiology, University of North Carolina at Chapel Hill, Chapel Hill, NC, USA. [5]Department of Integrative Structural and Computational Biology, The Scripps Research Institute, La Jolla, CA, USA. [6]Division of Infectious Diseases, Department of Medicine, University of California San Diego, La Jolla, CA, USA. [7]Skaggs Institute for Chemical Biology, The Scripps Research Institute, La Jolla, CA, USA. [8]Department of Computer Science, Johns Hopkins University, Baltimore, MD, USA. [9]Departments of Microbiology and Immunology, University of North Carolina at Chapel Hill, Chapel Hill, NC, USA. [10]Ragon Institute of Massachusetts General Hospital, Massachusetts Institute of Technology and Harvard University, Cambridge, MA, USA. [11]These authors contributed equally: Wan-ting He, Rami Musharrafieh, Ge Song, Katharina Dueker. ✉e-mail: rbaric@email.unc.edu; lgralins@email.unc.edu; burton@scripps.edu; andrabi@scripps.edu

Results

Donors for bnAb isolation. To identify donors for bnAb isolation, we first screened sera from three different groups for SARS-CoV-2 neutralization. The groups were: (1) donors convalescing from COVID-19 ($n=21$); (2) spike mRNA-vaccinated (2×) donors ($n=10$); and (3) donors convalescing from COVID-19 ($n=15$) who had subsequently been mRNA-vaccinated (1×) (Fig. 1a and Extended Data Fig. 1). Consistent with earlier studies, we observed significantly higher levels of plasma nAbs in donors who were previously infected and then vaccinated ('recovered vaccinated') compared to donors who were only infected or only vaccinated (Fig. 1a and Extended Data Fig. 1). To examine the breadth of nAb responses across these three groups, we tested sera for neutralization against ACE2 receptor-utilizing sarbecoviruses (Pang17, SARS-CoV-1 and WIV1) and against SARS-CoV-2 VOCs (B.1.1.7 (Alpha), B.1.351 (Beta), P.1 (Gamma), B.1.617.2 (Delta) and B.1.1.529 (Omicron)) (Fig. 1b,c and Extended Data Fig. 1). Sera from recovered vaccinated donors showed greater breadth of neutralization and more effective neutralization of VOCs than sera from donors who were only previously infected or only vaccinated. Consistent with previous studies, the neutralization efficacy of recovered vaccinated sera against VOCs was similar to that against the ancestral strain of SARS-CoV-2 (refs. [32,36,41,42]) (Fig. 1c and Extended Data Fig. 1). Neutralization of SARS-CoV-1, whose spike is phylogenetically distinct (approximately 15% divergent at the amino acid level) from SARS-CoV-2 (refs. [14,43]), was relatively low but was clearly above background for about half of the recovered vaccinated donors (Extended Data Fig. 1). None of the convalescent-only or vaccinated-only donor sera could neutralize SARS-CoV-1, as noted by us in an earlier study[44]. Of note, many of the existing SARS-CoV-2 cross-reactive or cross-nAbs were isolated from convalescent donors with SARS-CoV-1 (refs. [15,20,45–48]) and only more recently from donors infected with SARS-CoV-2 (refs. [18,19,22,23,49]). BnAbs have also been isolated from SARS-CoV-2 spike protein-vaccinated macaques that showed serum cross-neutralizing activity against SARS-CoV-1 (refs. [44,50–52]). Hence, SARS-CoV-1/2 cross-neutralization appears to be a good indicator of the presence of pan-sarbecovirus activity and greater coronavirus neutralization breadth[53]. Accordingly, to isolate bnAbs in this study, we focused on two vaccinated donors who had recovered from SARS-CoV-2 infection (CC25 and CC84) with the most potent SARS-CoV-1 cross-neutralizing antibody titers.

Isolation and characterization of sarbecovirus bnAbs. Using SARS-CoV-1 and SARS-CoV-2 spike proteins as baits, we sorted antigen-specific single B cells to isolate 107 monoclonal antibodies (mAbs) from 2 donors who had recovered from COVID-19 and who had been recently vaccinated with the Moderna mRNA-1273 vaccine (CC25, $n=56$; CC84, $n=51$) (Extended Data Fig. 1) (ref. [54]). Briefly, from the peripheral blood mononuclear cells (PBMCs) of the donors, we sorted $CD19^+CD20^+$ IgG^+ IgM^- B cells that bound to both SARS-CoV-2 and SARS-CoV-1 spike proteins (Fig. 1d and Extended Data Fig. 1). Flow cytometry profiling of pre-vaccination (postinfection) PBMCs of donors CC25 and CC84 revealed that SARS-CoV-1/2 cross-reactive IgG^+ B cells were likely seeded after infection and were recalled on vaccination (Fig. 1d,e and Extended Data Fig. 1), as observed in other studies[32,55]. Heavy (HC) and light chain (LC) sequences from 107 spike protein sorted single B cells were recovered and expressed as IgGs (Extended Data Fig. 2).

All 107 mAbs exhibited cross-reactive ELISA binding to the SARS-CoV-2 and SARS-CoV-1 spike proteins (Fig. 2a and Extended Data Fig. 2). Very few of the mAbs showed weak but detectable binding to human betacoronavirus (β-HCoV) (Middle East respiratory syndrome coronavirus (MERS-CoV), HCoV-HKU1 and HCoV-OC43) and human alphacoronavirus (α-HCoV) (HCoV-NL63 and HCoV-229E)-derived spike proteins (Fig. 2a and Extended Data Fig. 2). To determine the epitope specificities of the mAbs, we tested ELISA binding with the SARS-CoV-2 S1 subunit domains and observed that the vast majority of mAbs (>80%) displayed RBD-specific binding (Fig. 2a). To determine the cross-reactivity of RBD binding, we investigated 12 diverse RBDs representing all the 4 major sarbecovirus clades: clades 1a, 1b, 2 and 3 (refs. [14,15,43]) (Fig. 2b and Extended Data Fig. 2). The mAbs showed the greatest degree of cross-reactivity with clades 1a and 1b and the least with clade 2. Approximately a third of the mAbs (31%) showed cross-reactivity with all 12 RBDs derived from all 4 sarbecovirus clades (Fig. 2b and Extended Data Fig. 2).

Next, we evaluated cross-clade neutralization with mAb supernatants on a panel of clade 1a (SARS-CoV-1 and WIV1) and clade 1b (SARS-CoV-2 and Pang17) pseudoviruses of ACE2-utilizing sarbecoviruses[14]. Two-thirds of mAbs neutralized both SARS-CoV-1 and SARS-CoV-2 and 43% (40 out of 93 mAbs) neutralized all 4 sarbecoviruses in the panel and are categorized as bnAbs in this study (Fig. 2b and Extended Data Fig. 2). More comprehensive and quantitative cross-neutralization with a smaller panel of mAbs is described below.

Regarding antibody sequences, of the 107 isolated mAbs, 93 were encoded by unique immunoglobulin germline-gene combinations and 11 were expanded lineages (CC25, $n=6$; CC84, $n=5$) that had 2 or more clonal members (Fig. 2a and Extended Data Fig. 2). There was a notable enrichment of immunoglobulin HC variable (*IGHV*) 3–30, particularly, and also the *IGHV* 1–46 and *IGHV* 1–69 germline gene families for both donors compared to human baseline germline frequencies (Fig. 2a,c,d and Extended Data Fig. 3) (refs. [56,57]). LCs of certain germline gene families (*IGKV* 1–33, *IGKV* 2–30, *IGLV* 1–40, *IGLV* 3–21) were also modestly enriched in the isolated mAbs (Extended Data Fig. 3). Interestingly, mAbs showed modest levels of V-gene nucleotide somatic hypermutation (SHM): VH, median = 5.0%; VL, median = 4.0% (Extended Data Fig. 2). Since multiple studies have shown that HCs dominate the epitope interaction by RBD nAbs[9,58–60], we sought to determine whether the *IGHV* germline gene usage and/or *VH* SHM levels were correlated with the extent of neutralization breadth (Fig. 2a,c,d). We observed enrichment of *IGHV* 3–30 in mAbs that bind to clade 2 RBDs and all 12 sarbecovirus RBDs, but otherwise no notable trends (Fig. 2c,d). VH-gene SHM levels did not distinguish potent broadly neutralizing from less broad or non-neutralizing mAbs. Overall, we observed that some *IGHV* or *IGLV* genes were enriched in bnAbs and several human immunoglobulin–gene combinations could encode for sarbecovirus bnAbs.

To further investigate the potential contribution of SHM to broad reactivity to sarbecoviruses, we tested the binding of mAbs to SARS-CoV-2 spike protein and to monomeric RBD by biolayer interferometry (BLI) (Extended Data Fig. 4). We found no association of SHM with spike protein binding and a weak correlation with binding to RBD. Consistent with this lack of correlation, we did not observe any correlation of SARS-CoV-2 RBD mAb binding with sarbecovirus neutralization breadth or binding breadth, although some modest correlation was observed for spike protein binding (Extended Data Fig. 4). These results suggest that critical antibody paratope features for sarbecovirus breadth when targeting the sites described below may be germline-encoded and limited affinity maturation is needed. While recent findings demonstrate that the accumulation of SHM may increase potency and breadth[38,61], this may not be a requisite feature of sarbecovirus bnAbs, as noted by others[62]. The predominant use of certain germline gene segments in bnAbs suggests that a germline-targeting approach[27–29] to pan-sarbecovirus vaccines may be rewarding; the relatively low levels of SHM are promising for successful vaccine deployment provided appropriate immunogens can be designed.

Next, we examined the complementarity determining region (CDR) H3 loop lengths of the isolated Abs and observed a strong

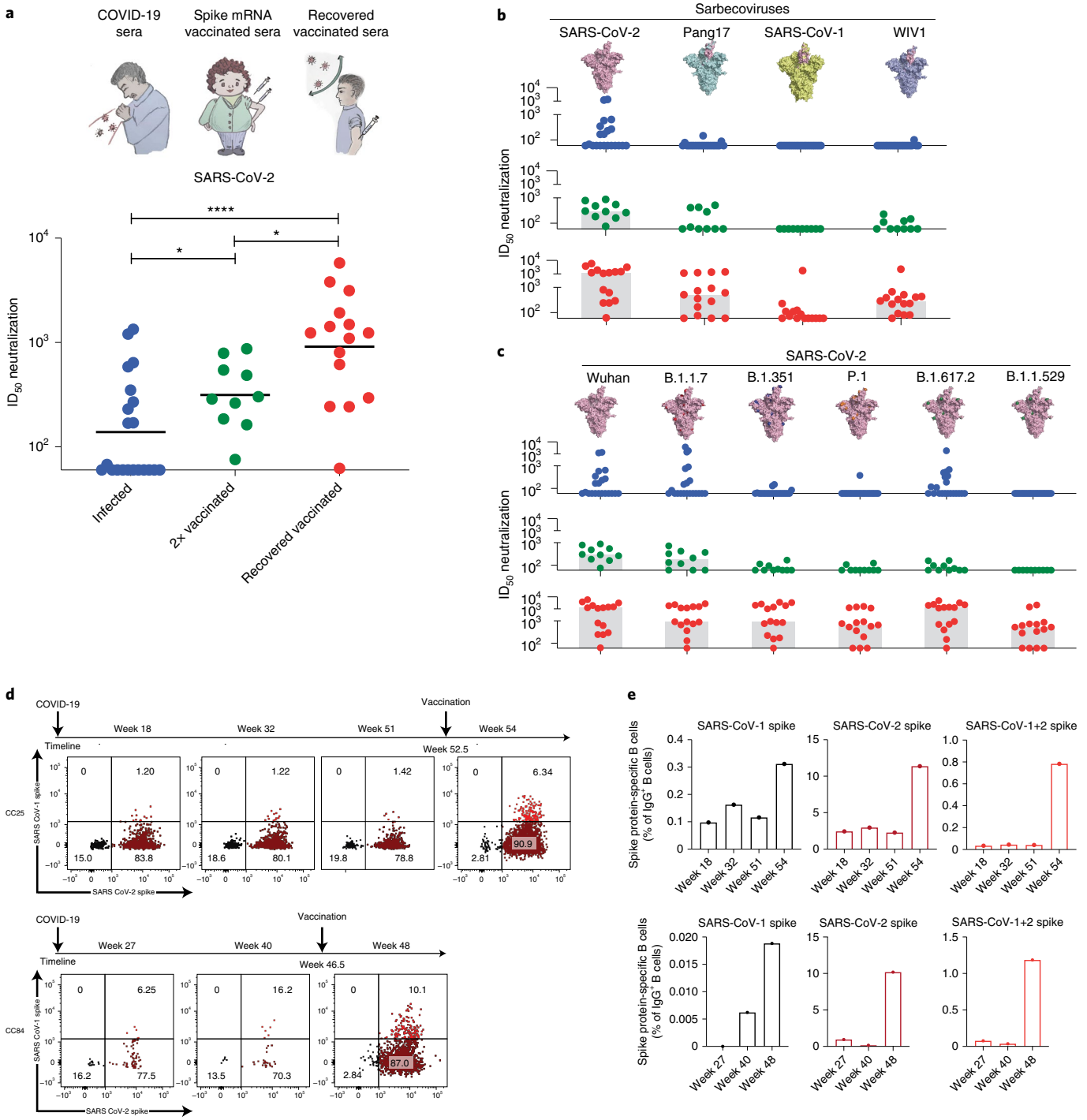

Fig. 1 | Plasma neutralization and B cell responses in convalescent recovered, vaccinated and recovered vaccinated donors. a, SARS-CoV-2 pseudovirus neutralization of plasma samples from convalescent donors who had recovered from COVID-19 (blue, recovered), vaccinated donors (green, 2×vaccinated) or vaccinated donors with a previous history of SARS-CoV-2 infection (red, recovered vaccinated). Donors who had recovered from COVID-19 ($n=21$), spike mRNA-vaccinated (2×) donors ($n=10$) and vaccinated donors who had recovered from COVID-19 ($n=15$) are shown. Data are shown as scatter dot plots with a line at the geometric mean value. Statistical comparisons between the two groups were performed using a two-tailed Mann–Whitney *U*-test (*$P<0.05$, ****$P<0.0001$). **b**, Plasma neutralization for all three groups against distantly related sarbecoviruses. Pang17 (cyan), SARS-CoV-1 (yellow) and WIV1 (violet) are shown. RBDs are colored pink for all spikes. In contrast to infected-only and vaccinated-only donors, approximately half of recovered vaccinated donors had neutralizing titers against SARS-CoV-1 above background (Extended Data Fig. 1). Data are shown as scatter dot plots; the bar height represents the median. **c**, Plasma neutralizing activity against SARS-CoV-2 (Wuhan) and SARS-CoV-2 variants of concern (B.1.1.7 (Alpha), B.1.351 (Beta), P.1 (Gamma), B.1.617.2 (Delta) and B.1.1.529 (Omicron)). Data are shown as scatter dot plots; the bar height represents the median. **d**, Flow cytometry analysis of IgG$^+$ B cells from the PBMCs of human donors CC25 and CC84 isolated at the indicated time points (see Extended Data Fig. 2 for the gating strategy). The numbers indicate the percentage of cells binding to SARS-CoV-1 and SARS-CoV-2 spike proteins, respectively. **e**, Quantification of SARS-CoV-1-specific, SARS-CoV-2-specific and cross-reactive IgG$^+$ B cells from donor CC25 (top) and donor CC84 (bottom).

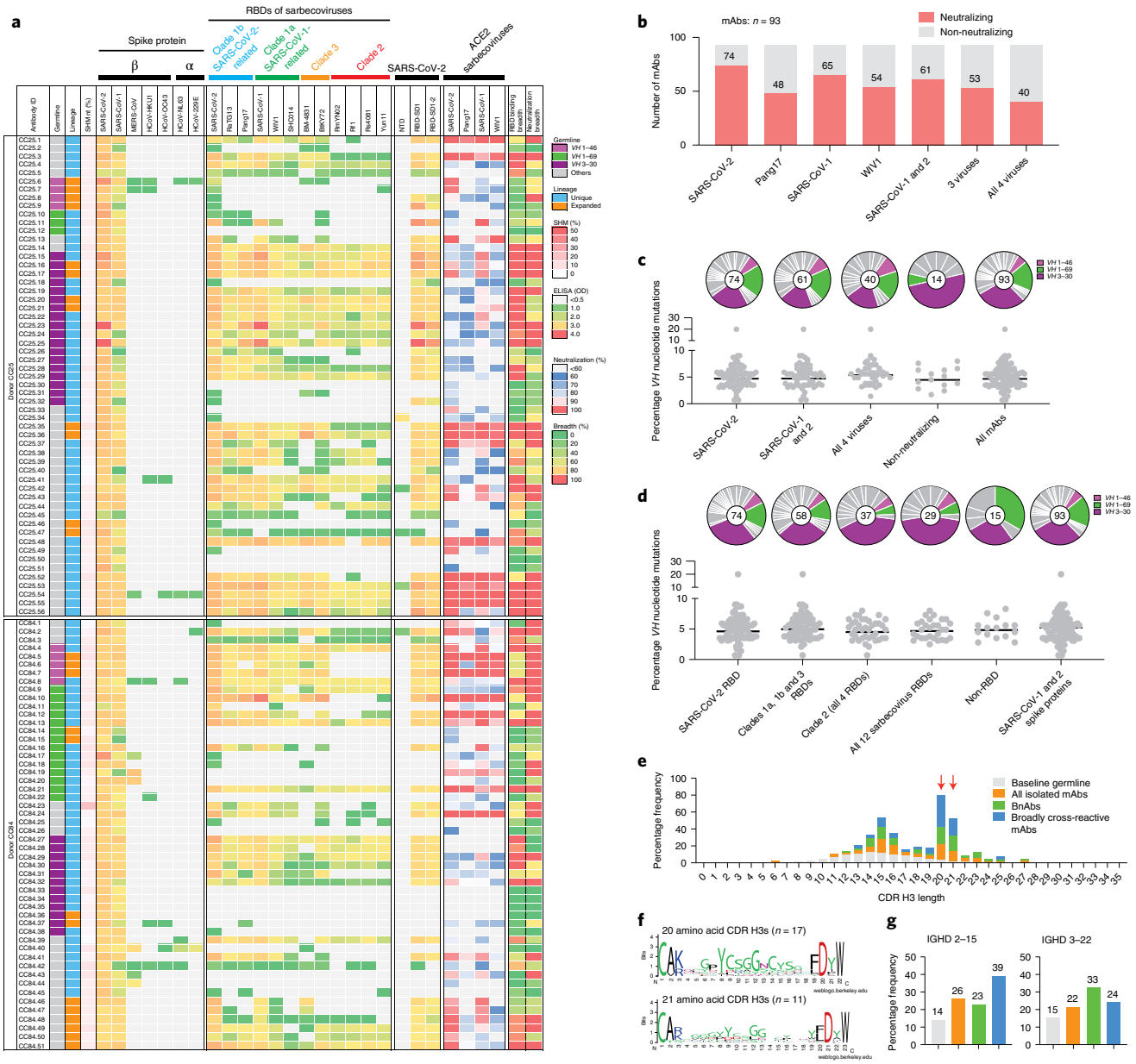

Fig. 2 | Binding, neutralization and immunogenetic properties of sarbecovirus mAbs. A total of 107 mAbs were isolated, 56 mAbs from donor CC25 and 51 mAbs from donor CC84. MAbs were isolated by single B cell sorting using SARS-CoV-1 and SARS-CoV-2 spike proteins as baits. **a**, Heatmap showing *IGHV* germline gene usage (*IGVH* 1–46 (magenta); *IGVH* 1–69 (green); *IGVH* 3–30 (plum); and other V genes (gray)), lineage information (unique (sky) and expanded (tangerine) lineages) and V-gene SHMs. ELISA binding activity of mAbs with SARS-CoV-2, SARS-CoV-1 and other β- and α-HCoV-derived spike proteins and domains of the SARS-CoV-2 spike protein (NTD, RBD-SD1 and RBD-SD2) (limit of detection < 0.5, optical density at 405 nm). Binding of mAbs with clade 1a (SARS-CoV-2-related: SARS-CoV-2, RatG13, Pang17), clade 1b (SARS-CoV-1-related: SARS-CoV-1, WIV1, SHC014), clade 2 (RmYN02, Rf1, Rs4081, Yun11) and clade 3 (BM-4831, BtKY72) sarbecovirus spike protein-derived monomeric RBDs. Percentage neutralization of ACE2-utilizing sarbecoviruses (SARS-CoV-2, Pang17, SARS-CoV-1 and WIV1) by mAb supernatants (cutoff < 60%). Breadth (%) of binding to 12 sarbecovirus RBDs and breadth (%) of neutralization with 4 ACE2 sarbecoviruses is indicated for each mAb. MAb expression levels in the supernatants were quantified by total IgG ELISA; the concentrations were approximately comparable overall. For reproducibility, the binding and neutralization assays were all performed twice with mAb supernatants expressed independently twice. **b**, Number of mAbs (unique clones) neutralizing SARS-CoV-2 and other sarbecoviruses. Forty mAbs neutralized all 4 ACE2 sarbecoviruses tested. **c**, Pie plots showing *IGHV* gene usage distribution of isolated mAbs ($n = 93$) with enriched gene families colored: *IGVH* 1–46 (magenta); *IGVH* 1–69 (green); and *IGVH* 3–30 (plum). The dot plots show the percentage of SHMs in the HC of isolated mAbs. SHMs are shown as scatter dot plots with a line at the geometric mean. MAbs are grouped by neutralization with sarbecoviruses. **d**, Pie and dot plots depicting *IGHV* gene distribution and HC nucleotide SHMs, respectively. MAbs ($n = 93$) are grouped by binding to sarbecovirus-derived RBDs. SHMs are shown as scatter dot plots with a line at the geometric mean. **e**, CDR H3 length distributions of isolated mAbs ($n = 93$) across broadly neutralizing and broadly cross-reactive mAb groups compared to the human baseline germline reference. MAbs with 20- and 21-amino acid CDR H3 loops are highly enriched. **f**, Sequence conservation logos of 20 ($n = 17$) and 21 ($n = 11$) amino-acid-long CDR H3-bearing mAbs showing enrichment of D-gene-derived residues, including the *IGHD* 2–15 germline D-gene, encoded 2 cysteines in 20 amino-acid-long CDR H3-bearing mAbs that may potentially form a disulfide bond. **g**, Enrichment of *IGHD* 2–15 and *IGHD* 3–22 germline D-genes in sarbecovirus broadly neutralizing or broadly cross-reactive mAbs compared to the corresponding human baseline germlines.

enrichment for 20- and 21-residue-long CDR H3 loops compared to the human baseline reference database (Fig. 2e)[56,57]. These long CDR H3 loops contained high proportions of two D-genes, *IGHD* 2–15 and *IGHD* 3–22, which were notably enriched in bnAbs (Fig. 2g). Notably, 71% (12 out of 17) of mAbs with 20-amino-acid CDR H3 loops utilized the germline *IGHD* 2–15 D-gene; most mAbs bearing 21-amino-acid CDR H3 loops utilized either the *IGHD* 2–15 or *IGHD* 3–22 germline D-genes (Fig. 2f and Extended Data Figs. 2 and 3). We noted that the *IGHD* 3–22 D-gene was also selected in bnAbs isolated in other studies[19,49,63,64]. Therefore, vaccine design strategies will likely need to take these germline features into consideration[27–29].

Altogether, we isolated a large panel of human sarbecovirus bnAbs. The isolated bnAbs, although encoded by several immunoglobulin germline gene families, are strongly enriched for certain germline gene features that will inform pan-sarbecovirus vaccine strategies.

Detailed binding and neutralization of selected bnAb panel. We selected 30 SARS-CoV-1/SARS-CoV-2 RBD cross-reactive mAbs for more detailed characterization (Fig. 3a). Selection of mAbs was made based on a high degree of cross-reactive binding with RBDs of multiple sarbecovirus clades. The large panel above included nAbs that likely had more potent neutralization of SARS-CoV-1 and/or SARS-CoV-2 individually but lacked broad binding activity (Fig. 2a). To determine sarbecovirus binding cross-reactivity more extensively, we evaluated 12 soluble monomeric RBDs representing the major sarbecovirus clades, as in Fig. 2. Almost all mAbs bound SARS-CoV-2 and other clade 1b-derived RBDs, with most binding in a nanomolar (nM) to picomolar (pM) *Kd* affinity range (Fig. 3b and Extended Data Fig. 5). The mAbs that bound most effectively to clade 1b RBDs tended to also bind well to clade 1a and clade 3 RBDs, albeit with somewhat lower affinities, yet still in the nM–pM *Kd* affinity range. Cross-reactive binding was least to the clade 2 RBDs, although there was generally some level of reactivity and some mAbs showed high affinity binding to clade 2 RBDs. Remarkably, several mAbs showed consistently high affinity binding to RBDs from all four sarbecovirus clades (Fig. 3b and Extended Data Fig. 5).

Neutralization was investigated only for clade 1a and 1b ACE2-utilizing viruses because neutralization assays were not available for clade 2 and 3 viruses. Twenty-two of 30 mAbs neutralized SARS-CoV-2 with a range of half-maximal inhibitory concentration (IC_{50}) neutralization titers (IC_{50} range = 0.05–4.9 μg ml^{-1}) (Fig. 3c) and 28 of 30 mAbs neutralized SARS-CoV-1, including all mAbs that neutralized SARS-CoV-2. Neutralization potency was typically stronger against SARS-CoV-1 than SARS-CoV-2. All mAbs showed neutralization against WIV1, while a majority exhibited cross-neutralization with Pang17 and to a lesser degree with SHC014. Thirteen out of 30 mAbs neutralized all 5 ACE2-utilizing sarbecoviruses tested with a geometric mean IC_{50} potency of 0.12 μg ml^{-1}. The 3 most potent SARS-CoV-2 bnAbs, CC25.52, CC25.54 and CC25.3, neutralized all 5 ACE2-utilizing sarbecoviruses with geometric mean potencies of 0.03, 0.04 and 0.04 μg ml^{-1}, respectively. Although neutralization assays differ, this suggests they are among the most potent and broad individual nAbs described to date (also compare control nAbs in Fig. 3c).

We tested the neutralization of SARS-CoV-2 VOCs by 20 select SARS-CoV-2 bnAbs. Consistent with the donor CC25 and CC84 sera neutralization above, the bnAbs were consistently effective against the SARS-CoV-2 VOCs tested (Fig. 3d and Extended Data Fig. 6). The IC_{50} neutralization titers of bnAbs were largely unchanged against the Alpha, Beta, Gamma and Delta SARS-CoV-2 VOCs but were more affected by substitutions in the Omicron variant (Fig. 3d and Extended Data Fig. 6). Nevertheless, IC_{50} neutralization titers for many bnAbs were unchanged or minimally affected for the Omicron variant; remarkably, 14 of 20 bnAbs retained substantial neutralization against this highly evolved SARS-CoV-2 variant (Fig. 3d and Extended Data Fig. 6). In comparison, the SARS-CoV-2 strain-specific nAb CC12.1 showed substantial or complete loss of neutralization with VOCs. The results suggest that these bnAbs target more conserved RBD epitopes, which are likely more resistant to SARS-CoV-2 escape mutations. Overall, we identified multiple potent sarbecoviruses bnAbs that exhibit broad reactivity to SARS-CoV-2 variants and diverse sarbecovirus lineages.

Epitope specificity of sarbecovirus bnAbs. To help map the epitopes recognized by the sarbecovirus bnAbs, we first epitope-binned them using BLI competition with RBD nAbs of known specificities (Fig. 4a and Extended Data Fig. 7), including 5 human nAbs: (1) CC12.1, a receptor binding site (RBS)-A or class 1 nAb targeting the ACE2 binding site[9,59,65]; (2) CC12.19, which is thought to recognize a complex RBD epitope and competes with some non-RBD Abs[66]; (3) CR3022, which recognizes the class 4 epitope site[9,65]; (4) S309, which recognizes the class 3 epitope site[9,65]; and (5) DH1047, which recognizes a conserved site and is class 4[20]. In addition, we included K398.22, a macaque bnAb[44], which targets an RBD bnAb epitope distinct from that recognized by human bnAbs characterized to date but has features characteristic of class 4 bnAbs (Fig. 4a,b). The bnAbs we describe in this study can be clustered for convenience into two major groups. Group 1 bnAbs strongly competed with the SARS-CoV-2 class 4 human bnAbs, CR3022 and DH1047, and macaque bnAb K398.22, showed more sporadic competition with CC12.1 and did not compete with CC12.19 or S309. Group 2 mAbs competed strongly with CC12.19, weakly with macaque K398.22 and only infrequently and/or weakly with any of the other bnAbs. Group 1 bnAbs were potent and broad in their neutralization of ACE2-utilizing sarbecoviruses but many lineage members displayed limited binding reactivity with clade 2 sarbecovirus RBDs. Group 2 mAbs showed broader binding reactivity with sarbecoviruses but were relatively less potent compared to group 1 bnAbs (Fig. 4a). Notably, 1 group 2 bnAb, CC25.11, showed strong competition with human class 3 RBD bnAb, S309, and the macaque bnAb, K398.22 (ref. [44]). The findings suggest that both group 1 and 2 bnAbs target more conserved RBD epitopes but group 1 bnAbs are overall more potent but less broad against clade 2 sarbecoviruses, with some exceptions.

To further investigate the epitopes recognized by the bnAbs, we utilized single-particle, negative stain electron microscopy and confirmed that the nine group 1 and two group 2 bnAb Fabs bound to the RBD of the SARS-CoV-2 spike protein (Fig. 4c and Extended Data Fig. 8). The binding modes of bnAbs to the SARS-CoV-2 spike protein were largely similar with some differences in the angles of approaches but not distinct enough to clearly segregate group 1 epitope bnAbs. Furthermore, structural studies that reveal molecular details of the antibody–antigen interactions contributing to the differences in epitope recognition are important. The group 2 bnAb reconstructions are consistent with an epitope that spans the RBD and other parts of the spike protein as described for the competitive Ab CC12.19 (ref. [66]). These bnAb Fabs showed binding to spike protein with all three stoichiometries (trimer 1:1, 1:2 and 1:3) with some of the Fabs exhibiting destabilizing effects on the spike trimer; this destabilization is seen as dimers and flexible densities in the two-dimensional (2D) class averages (Fig. 4c and Extended Data Figs. 8 and 9). Based on the antibody competitions, the putative epitope regions targeted by the group 1 RBD bnAbs are conserved across sarbecovirus RBDs (Fig. 4d, e).

Immunogenetics of groups 1 and 2 RBD bnAbs and vaccine targeting. To further understand the differences between group 1 and 2 RBD bnAbs and determine if germline gene features can differentiate their epitope properties, we performed detailed antibody

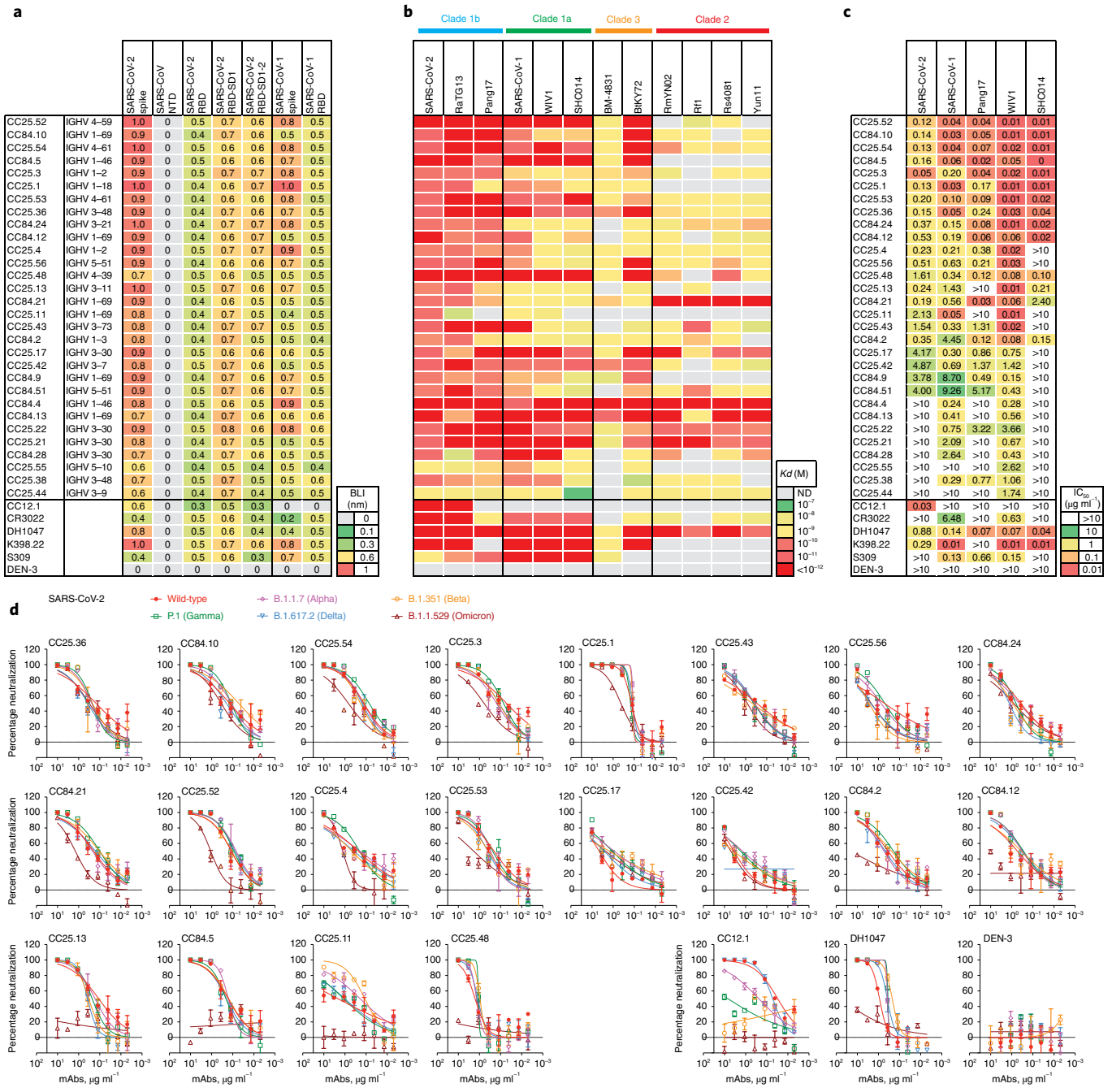

Fig. 3 | Binding and neutralization of mAbs in terms of affinity, potency and breadth. A total of 19 mAbs from donor CC25 and 11 mAbs from donor CC84 were selected to determine specificity, relative affinities and neutralization of sarbecoviruses and SARS-CoV-2 VOCs. **a**, Heatmap of binding responses (nM) determined by BLI using the SARS-CoV-1 and SARS-CoV-2 spike and S-protein domains and subdomains with *IGHV* gene usage for each mAb indicated. **b**, Heatmap of dissociation constants (*Kd* (M) values) for mAb binding to spike-derived monomeric RBDs from 4 sarbecovirus clades: clade 1b ($n=3$); clade 1a ($n=3$); clade 2 ($n=4$); clade 3 ($n=2$). Binding kinetics were obtained using the 1:1 binding kinetics fitting model in the ForteBio Data Analysis software (version 12.0). **c**, IC_{50} neutralization of mAbs against SARS-CoV-2, SARS-CoV-1, Pang17, WIV1 and SHC014 determined using pseudotyped viruses. **d**, Neutralization of 20 bnAbs against SARS-CoV-2 (Wuhan) and 5 major SARS-CoV-2 variants of concern (B.1.1.7 (Alpha), B.1.351 (Beta), P.1 (Gamma), B.1.617.2 (Delta) and B.1.1.529 (Omicron)). The SARS-CoV-2 Abs, CC12.1 and DH1047, and the Dengue Ab, DEN-3, were used as controls. Data are presented as the mean ± s.d. The experiments were performed independently twice and consistent results were obtained.

immunogenetic analysis. Both groups of RBD bnAbs were encoded by a number of *IGHV* germline gene families (Fig. 5a). The average CDR H3 loop lengths were significantly longer ($P<0.05$) in group 1 compared to group 2 RBD bnAbs (Fig. 5b). Notably, group 1 bnAbs were strongly enriched (60%: 9 out of 15 group 1 RBD bnAbs) for *IGHD* 3–22 germline D-gene-encoded CDR H3 YYDxxG motifs and possessed significantly longer CDR H3 loops ($P<0.005$) compared to the other mAbs (Fig. 5c,d). The *IGHD* 3–22 germline D-gene YYDxxG motif-bearing group 1 RBD bnAbs utilized several *IGHV* germline gene combinations and the D-gene motifs were either retained in a germline configuration (YYDSSG: CC25.48 and CC84.2) or one or both 'X' residues were mutated (Fig. 5c,d,e). The

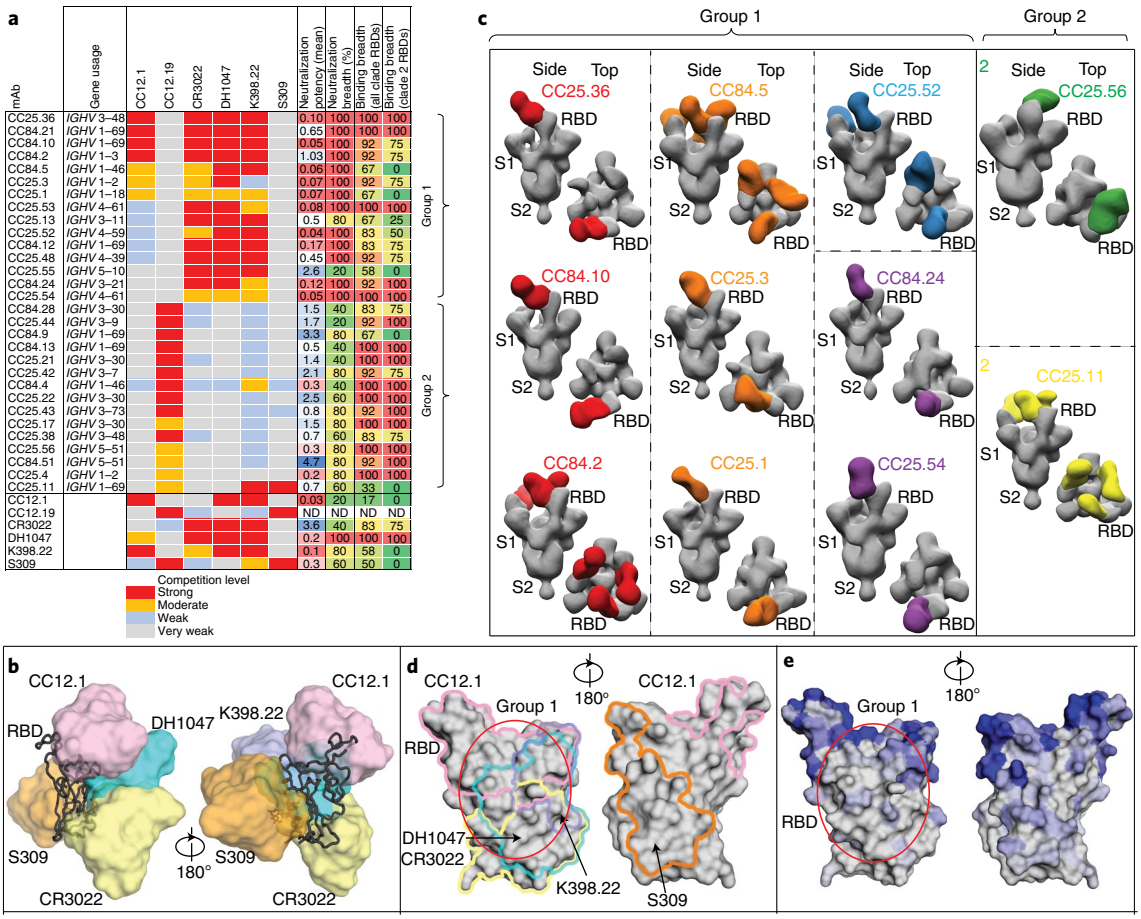

Fig. 4 | Epitope specificities of sarbecovirus bnAbs. a, Heatmap summary of epitope binning of sarbecovirus bnAbs based on BLI competition of bnAbs with human (CC12.1, CC12.19, CR3022, DH1047 and S309) and macaque (K398.22) RBD-specific nAbs. *IGHV* gene usage for each mAb is indicated. Geometric mean neutralization potency and breadth (calculated from Fig. 3c) and RBD binding breadth with clade 2 or all clade sarbecoviruses (calculated from Fig. 3b) for each mAb are indicated. BLI competition was performed with monomeric SARS-CoV-2 RBD; competition levels are indicated as red (strong), orange (moderate), light blue (weak) and gray (very weak) competition. Based on competition with human and one macaque nAb of known specificities, sarbecovirus bnAbs were divided into groups 1 and 2. **b**, Binding of human nAbs to SARS-CoV-2 RBD. The RBD is shown as a black chain trace, whereas antibodies are represented by solid surfaces in different colors: CC12.1 (pink, Protein Data Bank (PDB) ID: 6XC2), CR3022 (yellow, PDB ID: 6W41), S309 (orange, PDB ID: 7R6W), DH1047 (cyan, PDB ID: 7LD1) and K398.22 (blue, PDB ID: 7TP4) (ref. [44]). **c**, Electron microscopy three-dimensional (3D) reconstructions of sarbecovirus bnAb Fabs with SARS-CoV-2 spike protein. The Fabs of groups 1 ($n=9$) and 2 ($n=2$) were complexed with SARS-CoV-2 spike protein and 3D reconstructions were generated from 2D class averages. Fabs are shown in different colors; the spike S1 and S2 subunits (gray) and RBD sites are labeled. **d**, The epitope of each antibody is outlined in different colors corresponding to **b**. Epitope residues are defined by buried surface area > 0 Å^2 as calculated by PDBePISA (Proteins, Interfaces, Structures and Assemblies) (https://www.ebi.ac.uk/msd-srv/prot_int/pistart.html). Putative epitope regions of group 1 bnAbs based on the competitive binding assay are indicated by the red circle. **e**, Conservation of 12 sarbecovirus RBDs. The gray surface represents conserved regions, whereas blue represents variable regions. The conservation was calculated by ConSurf (https://consurf.tau.ac.il/). The putative epitope region targeted by group 1 bnAbs is circled as in **d**.

most common mutation was the substitution of YYD-proceeding X residue, serine (S) to an arginine (R), which appeared recurrently in multiple YYDxxG motif-bearing RBD bnAbs from both donors suggesting common B cell affinity maturation pathways. Interestingly, the S-R somatic mutation in the CDR H3 YYDxxG motif was important for resisting Omicron neutralization escape since the nonmutated YYDxxG motif-bearing group 1 RBD bnAbs failed or weakly neutralized this variant (Fig. 5f and Extended Data Fig. 6). Consistent with this observation, recent studies provided evidence for how YYDRxG RBD bnAbs can effectively bind to the conserved face of SARS-CoV-2 spike RBD[67,68]. The findings reveal that RBD bnAbs with certain recurrent germline features can effectively resist SARS-CoV-2 Omicron escape (Extended Data Fig. 6) but several antibody solutions can counter this extreme antigenic shift and should be considered for vaccine targeting. Remarkably, in our study genetically diverse RBD bnAbs in both groups 1 and 2 effectively neutralized the Omicron variant (Extended Data Fig. 6) suggesting that several human antibody solutions can counter SARS-CoV-2 antigenic shift.

The association of a germline D-gene encoded motif provides an opportunity for broad vaccine targeting, as described for HIV[27,29,69]. For SARS-like coronaviruses, the YYDxxG motif[67,68] appears promising for vaccine targeting. Encouragingly, human naive B cell repertoires encode a sizable fraction of *IGHD3-22* germline D-gene-encoded YYDxxG motif-bearing B cells with desired CDR H3 lengths (Fig. 5g) that could be targeted by rationally designed vaccines[70].

RBD bnAbs protect against diversity of sarbecoviruses. To determine the protective efficacy of RBD bnAbs, we conducted passive

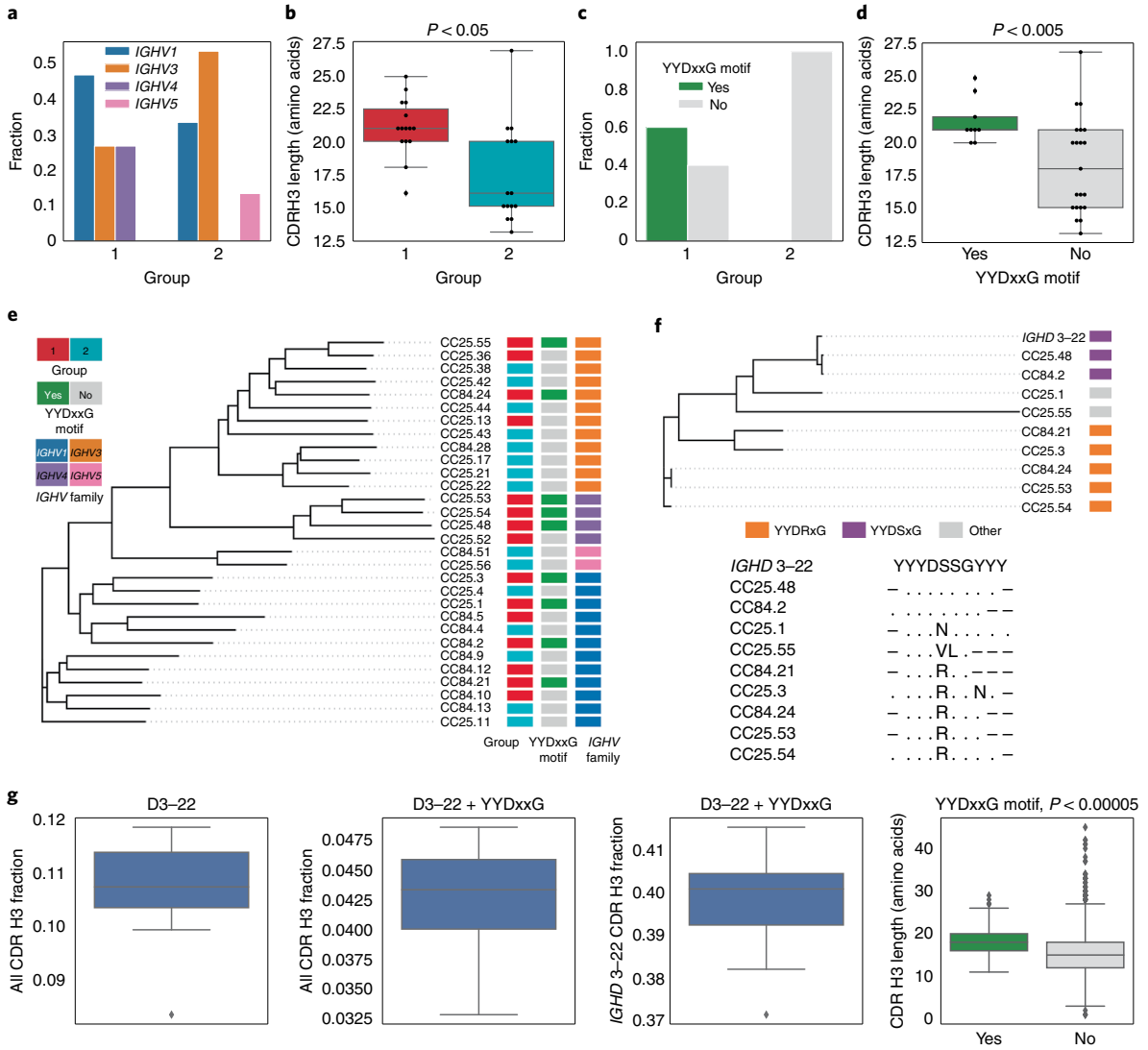

Fig. 5 | Immunogenetic properties of groups 1 and 2 RBD bnAbs. a, VH-gene family usage: *IGHV1* (blue), *IGHV3* (orange), *IGHV4* (violet) and *IGHV5* (pink). **b**, CDR H3 length distribution (amino acids) in groups 1 (red) and 2 (cyan) ($n = 30$). **c**, CDR H3 use of the YYDxxG motif in groups 1 and 2 RBD bnAbs: with (green) and without (gray) ($n = 30$). **d**, CDR H3 length distribution in RBD bnAbs with (green) and without (gray) YYDxxG motifs ($n = 30$). **e**, Phylogenetic tree of HC sequences of 30 RBD bnAbs. Each sequence is colored according to its group (left), *IGHV* gene family (middle) and the presence of the YYDxxD motif in the HCDR3 (right). The colors of the HC characteristics are consistent with **a**–**d**. The phylogenetic tree was computed using Clustal Omega (version 1.2.2, https://www.ebi.ac.uk/Tools/msa/clustalo)[80]. **f**, Phylogenetic tree combining *IGHD* gene fragments of CDR H3s of nine mAbs with YYDxxG motifs and amino acid translation of the germline sequence of *IGHD* 3-22-containing YYGSSG. Each sequence is colored according to the amino acid following YYD: S (violet), R (orange) or others (gray). The alignment corresponding to the tree is shown below it. The dots represent amino acids matching the germline amino acids. Germline amino acids truncated in CDR H3s are shown by dashes. **g**, Frequencies of *IGHD* 3-22 germline genes with differing characteristics in naive HC repertoires. Left to right: all *IGHD* 3-22 in all CDR H3s; *IGHD* 3-22 with YYDxxG motif in all CDR H3s; *IGHD* 3-22 with YYDxxG motif in CDR H3s derived from *IGHD* 3-22; distribution of lengths (in amino acids) of CDR H3s with (green) and without (gray) YYDxxG motifs. The fraction statistics were computed using ten repertoire sequencing libraries representing ten donors from the study by Gidoni et al.[81]: ERR2567178–ERR2567187. The distribution of CDR H3 lengths was computed for library ERR2567178. For panels, **b**, **d** and **g**, data are shown as box plots, where the box and the middle line represent the quartiles and the median of the distribution, respectively. The whiskers show the rest of the distribution, except for outliers identified using a function of the interquartile range implemented by the Seaborn package in Python (version 0.11.2) and shown as diamonds. Distributions containing less than 25 points are also shown as non-overlapping dots visualized over boxes. *P*-values computed using the Kruskal-Wallis test and denoted as follows: $^{*}P < 0.05$, $^{**}P < 0.005$, $^{****}P < 0.00005$.

antibody transfer followed by challenge with sarbecoviruses in aged mice[71]. We selected three of the broadest group 1 bnAbs—CC25.36, CC25.53 and CC25.54—and investigated their in vivo protective efficacy against SARS-CoV-2, SARS-CoV-1 and SHC014 sarbecoviruses in mice. SHC014 was chosen because it encodes extensive heterogeneity in the spike RBD, reduces mRNA SARS-CoV-2 polyclonal neutralization serum titers by approximately 300-fold[72] and replicates efficiently in mice[73]. Before the protection studies, we compared neutralization by RBD bnAbs of replication-competent viruses with that of pseudoviruses (Extended Data Fig. 9). Neutralization of replication-competent SARS-CoV-1 and SARS-CoV-2 by bnAbs was more effective (lower IC_{50} values) than the corresponding pseudoviruses. Neutralization of replication-competent and pseudovirus versions of SHC014 by bnAbs was approximately equivalent.

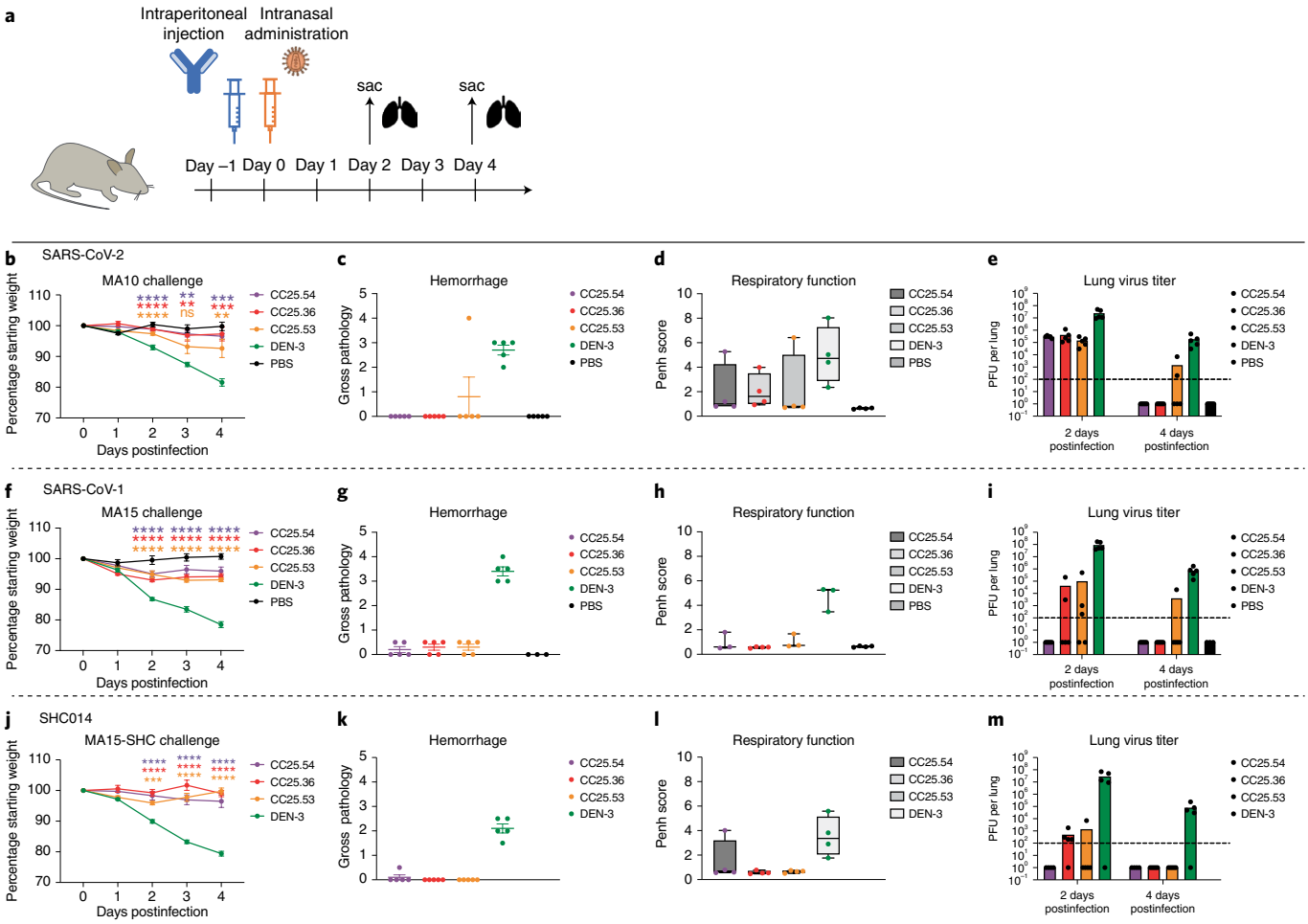

Fig. 6 | Prophylactic treatment of aged mice with RBD bnAbs protects against challenge. a, Three RBD bnAbs (CC25.54, CC25.36 and CC25.53) individually or a DEN-3 control antibody were administered intraperitoneally at 300 μg per animal into 12 groups of aged mice (10 animals per group). Each group of animals was challenged intranasally 12 h after antibody infusion with one of 3 MA sarbecoviruses (MA10, for SARS-CoV-2, 1×10^3 PFU; MA15 for SARS-CoV-1, 1×10^3 PFU; or MA15-SHC for the SARS-CoV MA15-SHC014 chimera, 1×10^5 PFU). As a control, groups of mice were exposed only to PBS in the absence of virus. **b**,**f**,**j**, Percentage weight change in RBD bnAbs or DEN-3 control antibody-treated animals after challenge with MA sarbecoviruses. Percentage weight change was calculated from the day 0 starting weight for all animals ($n=10$ individuals for each group were used). Data are presented as mean values ± s.e.m. Statistical significance was calculated with Dunnett's multiple comparisons test between each experimental group and the DEN-3 control Ab group. $^{**}P<0.01$, $^{***}P<0.001$, $^{****}P<0.0001$, NS $P>0.05$. NS, not significant. A one-way analysis of variance was used. **c**,**g**,**k**, Day 2 postinfection hemorrhage (gross pathology score) scored at tissue collection in mice prophylactically treated with RBD bnAbs or DEN-3 control mAb ($n=5$ individuals for each group). Data are presented as mean values ± s.e.m. **d**,**h**,**l**, Day 2 postinfection respiratory function (shown as Penh score) was measured by whole-body plethysmography in mice prophylactically treated with RBD bnAbs or DEN-3 control mAb ($n=5$ individuals for each group). Data are shown as box and whisker plots showing data points from minimum to maximum. **e**,**i**,**m**, Lung virus titers (PFU per lung) were determined by plaque assay of lung tissues collected at days 2 or 4 after infection ($n=5$ individuals per time point for each group). Data are shown as scatter dot plots with bar heights representing the mean.

The 3 RBD bnAbs individually or a Dengue virus 3 (DEN-3) control antibody were administered intraperitoneally at 300 μg per animal into 12 groups of 10 animals (3 groups per antibody; Fig. 6a). Each group was challenged with one of three mouse-adapted (MA) sarbecoviruses (MA10 for SARS-CoV-2, MA15 for SARS-CoV or MA15-SHC for the SARS-CoV MA15-SHC014 chimera), by intranasal administration of virus 12 h post-antibody infusion (Fig. 6a). Mice were monitored for signs of clinical disease due to infection, including daily weight changes and pulmonary function. Animals in each group were euthanized at day 2 or day 4 postinfection and lung tissues were collected to determine virus titers by plaque assay. Gross pathology was also assessed at the time of tissue collection. RBD bnAb-treated mice in all three sarbecovirus challenge experiments showed significantly reduced weight loss (Fig. 6b,f,j), reduced hemorrhage (Fig. 6c,g,k) and largely unaffected pulmonary function (Fig. 6d,h,l) compared to the DEN-3-treated control group mice, suggesting a protective role for bnAbs. We also examined virus load in the lungs at days 2 and 4 postinfection; consistent with the above results, both the day 2 and 4 viral titers in RBD bnAb-treated mice were substantially reduced compared to the DEN-3-treated control group mice (Fig. 6e,i,m). Overall, all three RBD bnAbs protected against severe sarbecovirus disease, CC25.54 and CC25.36 bnAbs being relatively more protective than CC25.53 bnAb. The animal data suggest potential utilization of the bnAbs in intervention strategies against diverse sarbecoviruses.

Discussion

In this study, we characterized a large panel of sarbecovirus bnAbs isolated from two vaccinated donors who had recovered from SARS-CoV-2. Select bnAbs showed robust in vivo protection against

diverse SARS-like viruses, including SARS-CoV-1, SARS-CoV-2 and SHC014, in a prophylaxis challenge model. The bnAbs were potent and showed neutralization of a range of VOCs; many were effective against the Omicron variant. The bnAbs recognized a relatively conserved face of the RBD that overlaps with the footprint of a number of antibodies including ADG 61123, DH1047 and CR302220 (refs. [46,68]) and broadly the face designated as that recognized by class 4 antibodies[9,60]. However, as illustrated in Fig. 4, the panel of bnAbs differed in many details of recognition, for instance, some compete with ACE2 while others do not; these differences are important in the resistance to mutations. As variants such as Omicron emerge during this and future coronavirus pandemics, the availability of a selection of potent bnAbs provides choice of optimal reagents for antibody-based interventions to respond to the viral threats.

In terms of vaccine design, the generation of HIV immunogens typically draws heavily on the availability of multiple bnAbs to a given site to provide the best input for design strategies[25,74]. The same consideration is likely to apply to pan-sarbecovirus vaccine design. Furthermore, although the bnAbs we isolated were encoded by several gene families, certain V- and D-gene families were highly enriched. We confirmed and identified specific antibody germline gene features associated with broad activity against diverse sarbecoviruses; vaccine design strategies may seek to target these genetic features by rationally designed prophylactic vaccines[25,27–29,70]. Some of the most potent bnAbs compete with the immunodominant human SARS-CoV-2 RBS-A/class 1 nAb CC12.1, which shows relatively low cross-reactivity. Elicitation of nAbs like CC12.1 may then reduce the elicitation of bnAbs; rational vaccine design modalities may need to mask RBS-A/class 1 immunodominant sites[75–77] while leaving the bnAb sites intact. Resurfaced RBD-based immunogens in various flavors[43,50–52] may achieve a similar goal.

Given the strong bnAb responses induced through infection-vaccination as indicated from serum studies and by our mAbs, are there lessons for vaccine design? The higher frequency of bnAbs in infection-vaccination may have a number of causes. First, the spike protein may have subtle conformational differences, particularly in the sites targeted by bnAbs, between the native structure on virions and the stabilized form presented by mRNA immunization. This may favor the activation of bnAbs in the infection step followed by recall during mRNA boosting. Second, the long time lag between infection and vaccination may have favored the accumulation of key mutations associated with bnAbs. There is evidence that intact HIV virions can be maintained on follicular dendritic cells in germinal centers over long time periods in a mouse model[78]. Third, T cell help provided by the infection may be superior to that provided by mRNA vaccination alone. Overall, there is an intriguing possibility that pan-sarbecovirus nAb activity may be best achieved by a hybrid approach[31] to immunization that seeks to mimic infection-vaccination, once the key contributing factors to breadth development in that approach can be determined. However, we also note that a very recent report described bnAbs arising from a third immunization with an inactivated vaccine[79].

In summary, we isolated multiple potent sarbecovirus protective cross-neutralizing human Abs and provide a molecular basis for broad neutralization. The bnAbs identified may themselves have prophylactic utility; the bnAb panel delineates the boundaries and requirements for broad neutralization and will be an important contributor to rational vaccine design.

Online content

Any methods, additional references, Nature Research reporting summaries, source data, extended data, supplementary information, acknowledgements, peer review information; details of author contributions and competing interests; and statements of data and code availability are available at https://doi.org/10.1038/s41590-022-01222-1.

Received: 7 January 2022; Accepted: 20 April 2022;
Published online: 2 June 2022

References

1. Baden, L. R. et al. Efficacy and safety of the mRNA-1273 SARS-CoV-2 vaccine. *N. Engl. J. Med.* **384**, 403–416 (2021).
2. Polack, F. P. et al. Safety and efficacy of the BNT162b2 mRNA Covid-19 vaccine. *N. Engl. J. Med.* **383**, 2603–2615 (2020).
3. Khoury, D. S. et al. Neutralizing antibody levels are highly predictive of immune protection from symptomatic SARS-CoV-2 infection. *Nat. Med.* **27**, 1205–1211 (2021).
4. Gilbert, P. B. et al. Immune correlates analysis of the mRNA-1273 COVID-19 vaccine efficacy trial. *Science* **375**, 43–50 (2022).
5. Earle, K. A. et al. Evidence for antibody as a protective correlate for COVID-19 vaccines. *Vaccine* **39**, 4423–4428 (2021).
6. Wang, P. et al. Antibody resistance of SARS-CoV-2 variants B.1.351 and B.1.1.7. *Nature* **593**, 130–135 (2021).
7. Mascola, J. R., Graham, B. S. & Fauci, A. S. SARS-CoV-2 viral variants—tackling a moving target. *JAMA* **325**, 1261–1262 (2021).
8. Wibmer, C. K. et al. SARS-CoV-2 501Y.V2 escapes neutralization by South African COVID-19 donor plasma. *Nat. Med.* **27**, 622–625 (2021).
9. Yuan, M. et al. Structural and functional ramifications of antigenic drift in recent SARS-CoV-2 variants. *Science* **373**, 818–823 (2021).
10. Harvey, W. T. et al. SARS-CoV-2 variants, spike mutations and immune escape. *Nat. Rev. Microbiol.* **19**, 409–424 (2021).
11. Lopez Bernal, J. et al. Effectiveness of Covid-19 vaccines against the B.1.617.2 (Delta) variant. *N. Engl. J. Med.* **385**, 585–594 (2021).
12. Abu-Raddad, L. J. et al. Effectiveness of the BNT162b2 Covid-19 vaccine against the B.1.1.7 and B.1.351 variants. *N. Engl. J. Med.* **385**, 187–189 (2021).
13. Menachery, V. D. et al. SARS-like WIV1-CoV poised for human emergence. *Proc. Natl Acad. Sci. USA* **113**, 3048–3053 (2016).
14. Letko, M., Marzi, A. & Munster, V. Functional assessment of cell entry and receptor usage for SARS-CoV-2 and other lineage B betacoronaviruses. *Nat. Microbiol.* **5**, 562–569 (2020).
15. Rappazzo, C. G. et al. Broad and potent activity against SARS-like viruses by an engineered human monoclonal antibody. *Science* **371**, 823–829 (2021).
16. Song, G. et al. Cross-reactive serum and memory B-cell responses to spike protein in SARS-CoV-2 and endemic coronavirus infection. *Nat. Commun.* **12**, 2938 (2021).
17. Zhou, P. et al. A human antibody reveals a conserved site on beta-coronavirus spike proteins and confers protection against SARS-CoV-2 infection. *Sci. Transl. Med.* **14**, eabi9215 (2022).
18. Jennewein, M. F. et al. Isolation and characterization of cross-neutralizing coronavirus antibodies from COVID-19^{+} subjects. *Cell Rep.* **36**, 109353 (2021).
19. Jette, C. A. et al. Broad cross-reactivity across sarbecoviruses exhibited by a subset of COVID-19 donor-derived neutralizing antibodies. *Cell Rep.* **36**, 109760 (2021).
20. Li, D. et al. In vitro and in vivo functions of SARS-CoV-2 infection—enhancing and neutralizing antibodies. *Cell* **184**, 4203–4219.e32 (2021).
21. Pinto, D. et al. Broad betacoronavirus neutralization by a stem helix-specific human antibody. *Science* **373**, 1109–1116 (2021).
22. Starr, T. N. et al. SARS-CoV-2 RBD antibodies that maximize breadth and resistance to escape. *Nature* **597**, 97–102 (2021).
23. Tortorici, M. A. et al. Broad sarbecovirus neutralization by a human monoclonal antibody. *Nature* **597**, 103–108 (2021).
24. Hurt, A. C. & Wheatley, A. K. Neutralizing antibody therapeutics for COVID-19. *Viruses* **13**, 628 (2021).
25. Andrabi, R., Bhiman, J. N. & Burton, D. R. Strategies for a multi-stage neutralizing antibody-based HIV vaccine. *Curr. Opin. Immunol.* **53**, 143–151 (2018).
26. Kwong, P. D. & Mascola, J. R. HIV-1 vaccines based on antibody identification, B cell ontogeny, and epitope structure. *Immunity* **48**, 855–871 (2018).
27. Andrabi, R. et al. Identification of common features in prototype broadly neutralizing antibodies to HIV envelope V2 apex to facilitate vaccine design. *Immunity* **43**, 959–973 (2015).
28. Jardine, J. et al. Rational HIV immunogen design to target specific germline B cell receptors. *Science* **340**, 711–716 (2013).
29. Steichen, J. M. et al. A generalized HIV vaccine design strategy for priming of broadly neutralizing antibody responses. *Science* **366**, eaax4380 (2019).
30. Bradley, T. et al. Antibody responses after a single dose of SARS-CoV-2 mRNA vaccine. *N. Engl. J. Med.* **384**, 1959–1961 (2021).
31. Crotty, S. Hybrid immunity. *Science* **372**, 1392–1393 (2021).
32. Goel, R. R. et al. Distinct antibody and memory B cell responses in SARS-CoV-2 naïve and recovered individuals following mRNA vaccination. *Sci. Immunol.* **6**, eabi6950 (2021).
33. Krammer, F. et al. Antibody responses in seropositive persons after a single dose of SARS-CoV-2 mRNA vaccine. *N. Engl. J. Med.* **384**, 1372–1374 (2021).

34. Reynolds, C. J. et al. Prior SARS-CoV-2 infection rescues B and T cell responses to variants after first vaccine dose. *Science* https://doi.org/10.1126/science.abh1282 (2021).
35. Saadat, S. et al. Binding and neutralization antibody titers after a single vaccine dose in health care workers previously infected with SARS-CoV-2. *JAMA* **325**, 1467–1469 (2021).
36. Stamatatos, L. et al. mRNA vaccination boosts cross-variant neutralizing antibodies elicited by SARS-CoV-2 infection. *Science* https://doi.org/10.1126/science.abg9175 (2021).
37. Turner, J. S. et al. SARS-CoV-2 mRNA vaccines induce persistent human germinal centre responses. *Nature* **596**, 109–113 (2021).
38. Wang, Z. et al. Naturally enhanced neutralizing breadth against SARS-CoV-2 one year after infection. *Nature* **595**, 426–431 (2021).
39. Schmidt, F. et al. High genetic barrier to SARS-CoV-2 polyclonal neutralizing antibody escape. *Nature* **600**, 512–516 (2021).
40. Tauzin, A. et al. A single dose of the SARS-CoV-2 vaccine BNT162b2 elicits Fc-mediated antibody effector functions and T cell responses. *Cell Host Microbe* **29**, 1137–1150.e6 (2021).
41. Edara, V. V. et al. Infection- and vaccine-induced antibody binding and neutralization of the B.1.351 SARS-CoV-2 variant. *Cell Host Microbe* **29**, 516–521.e3 (2021).
42. Bates, T. A. et al. Vaccination before or after SARS-CoV-2 infection leads to robust humoral response and antibodies that effectively neutralize variants. *Sci. Immunol.* **7**, eabn8014 (2022).
43. Cohen, A. A. et al. Mosaic nanoparticles elicit cross-reactive immune responses to zoonotic coronaviruses in mice. *Science* **371**, 735–741 (2021).
44. He, W.-T. et al. Broadly neutralizing antibodies to SARS-related viruses can be readily induced in rhesus macaques. Preprint at *bioRxiv* https://doi.org/10.1101/2021.07.05.451222 (2021).
45. Pinto, D. et al. Cross-neutralization of SARS-CoV-2 by a human monoclonal SARS-CoV antibody. *Nature* **583**, 290–295 (2020).
46. ter Meulen, J. et al. Human monoclonal antibody combination against SARS coronavirus: synergy and coverage of escape mutants. *PLoS Med.* **3**, e237 (2006).
47. Wec, A. Z. et al. Broad neutralization of SARS-related viruses by human monoclonal antibodies. *Science* **369**, 731–736 (2020).
48. Martinez, D. R. A broadly cross-reactive antibody neutralizes and protects against sarbecovirus challenge in mice. *Sci. Transl. Med.* **14**, eabj7125 (2022).
49. Liu, H. et al. Cross-neutralization of a SARS-CoV-2 antibody to a functionally conserved site is mediated by avidity. *Immunity* **53**, 1272–1280.e5 (2020).
50. Saunders, K. O. et al. Neutralizing antibody vaccine for pandemic and pre-emergent coronaviruses. *Nature* **594**, 553–559 (2021).
51. Walls, A. C. et al. Elicitation of potent neutralizing antibody responses by designed protein nanoparticle vaccines for SARS-CoV-2. *Cell* **183**, 1367–1382.e17 (2020).
52. Joyce, M. G. A SARS-CoV-2 ferritin nanoparticle vaccine elicits protective immune responses in nonhuman primates. *Sci. Transl. Med.* **14**, eabi5735 (2022).
53. Tan, C.-W. et al. Pan-sarbecovirus neutralizing antibodies in BNT162b2-immunized SARS-CoV-1 survivors. *N. Engl. J. Med.* **385**, 1401–1406 (2021).
54. Jackson, L. A. et al. An mRNA vaccine against SARS-CoV-2—preliminary report. *N. Engl. J. Med.* **383**, 1920–1931 (2020).
55. Mishra, P. K. et al. Vaccination boosts protective responses and counters SARS-CoV-2-induced pathogenic memory B cells. Preprint at *medRxiv* https://doi.org/10.1101/2021.04.11.21255153 (2021).
56. Soto, C. et al. High frequency of shared clonotypes in human B cell receptor repertoires. *Nature* **566**, 398–402 (2019).
57. Briney, B., Inderbitzin, A., Joyce, C. & Burton, D. R. Commonality despite exceptional diversity in the baseline human antibody repertoire. *Nature* **566**, 393–397 (2019).
58. Wang, Z. et al. mRNA vaccine-elicited antibodies to SARS-CoV-2 and circulating variants. *Nature* **592**, 616–622 (2021).
59. Yuan, M. et al. Structural basis of a shared antibody response to SARS-CoV-2. *Science* **369**, 1119–1123 (2020).
60. Barnes, C. O. et al. SARS-CoV-2 neutralizing antibody structures inform therapeutic strategies. *Nature* **588**, 682–687 (2020).
61. Muecksch, F. et al. Affinity maturation of SARS-CoV-2 neutralizing antibodies confers potency, breadth, and resilience to viral escape mutations. *Immunity* **54**, 1853–1868.e7 (2021).
62. Feldman, J. et al. Naive human B cells engage the receptor binding domain of SARS-CoV-2, variants of concern, and related sarbecoviruses. *Sci. Immunol.* **6**, eabl5842 (2021).
63. Brouwer, P. J. M. et al. Potent neutralizing antibodies from COVID-19 patients define multiple targets of vulnerability. *Science* **369**, 643–650 (2020).
64. Sakharkar, M. Prolonged evolution of the human B cell response to SARS-CoV-2 infection. *Sci. Immunol.* **6**, eabg6916 (2021).
65. Barnes, C. O. et al. Structures of human antibodies bound to SARS-CoV-2 spike reveal common epitopes and recurrent features of antibodies. *Cell* **182**, 828–842.e16 (2020).
66. Rogers, T. F. et al. Isolation of potent SARS-CoV-2 neutralizing antibodies and protection from disease in a small animal model. *Science* **369**, 956–963 (2020).
67. Liu, L. et al. An antibody class with a common CDRH3 motif broadly neutralizes sarbecoviruses. *Sci. Transl. Med.* **14**, eabn6859 (2022).
68. Liu, H. et al. A recurring YYDRxG pattern in broadly neutralizing antibodies to a conserved site on SARS-CoV-2, variants of concern, and related viruses. Preprint at *bioRxiv* https://doi.org/10.1101/2021.12.15.472864 (2021).
69. Gorman, J. et al. Structures of HIV-1 Env V1V2 with broadly neutralizing antibodies reveal commonalities that enable vaccine design. *Nat. Struct. Mol. Biol.* **23**, 81–90 (2016).
70. Burton, D. R. & Walker, L. M. Rational vaccine design in the time of COVID-19. *Cell Host Microbe* **27**, 695–698 (2020).
71. Leist, S. R. et al. A mouse-adapted SARS-CoV-2 induces acute lung injury and mortality in standard laboratory mice. *Cell* **183**, 1070–1085.e12 (2020).
72. Martinez, D. R. et al. Chimeric spike mRNA vaccines protect against *Sarbecovirus* challenge in mice. *Science* **373**, 991–998 (2021).
73. Menachery, V. D. et al. A SARS-like cluster of circulating bat coronaviruses shows potential for human emergence. *Nat. Med.* **21**, 1508–1513 (2015).
74. Burton, D. R. & Hangartner, L. Broadly neutralizing antibodies to HIV and their role in vaccine design. *Annu. Rev. Immunol.* **34**, 635–659 (2016).
75. Duan, H. et al. Glycan masking focuses immune responses to the HIV-1 CD4-binding site and enhances elicitation of VRC01-class precursor antibodies. *Immunity* **49**, 301–311.e5 (2018).
76. Hauser, B. M. et al. Rationally designed immunogens enable immune focusing following SARS-CoV-2 spike imprinting. *Cell Rep.* **38**, 110561 (2022).
77. Konrath, K. M. et al. Nucleic acid delivery of immune-focused SARS-CoV-2 nanoparticles drives rapid and potent immunogenicity capable of single-dose protection. *Cell Rep.* **38**, 110318 (2022).
78. Smith, B. A. et al. Persistence of infectious HIV on follicular dendritic cells. *J. Immunol.* **166**, 690–696 (2001).
79. Wang, K. et al. Memory B cell repertoire from triple vaccinees against diverse SARS-CoV-2 variants. *Nature* **603**, 919–925 (2022).
80. Sievers, F. et al. Fast, scalable generation of high-quality protein multiple sequence alignments using Clustal Omega. *Mol. Syst. Biol.* **7**, 539 (2011).
81. Gidoni, M. et al. Mosaic deletion patterns of the human antibody heavy chain gene locus shown by Bayesian haplotyping. *Nat. Commun.* **10**, 628 (2019).

Methods

Convalescent COVID-19 and human vaccinee sera. Sera from convalescent COVID-19 donors[17], spike mRNA-vaccinated humans and from vaccinated donors who had recovered from COVID-19, were provided through the Collection of Biospecimens from Persons Under Investigation for 2019-Novel Coronavirus Infection to Understand Viral Shedding and Immune Response Study (University of California San Diego (UCSD) institutional review board no. 200236). The protocol was approved by the UCSD Human Research Protection Program. Convalescent serum samples were collected based on COVID-19 diagnosis regardless of sex, race, ethnicity, disease severity or other medical conditions. All human donors were assessed for medical decision-making capacity using a standardized, approved assessment, and voluntarily gave informed consent before being enrolled in the study. A summary of demographic information of COVID-19 convalescent and vaccinated donors is listed in Supplementary Table 1.

Plasmid construction. To generate soluble spike ectodomain proteins from SARS-CoV-1 (residues 1–1,190; GenBank ID: AAP13567) and SARS-CoV-2 (residues 1–1,208; GenBank ID: MN908947), we constructed the expression plasmids by synthesizing the DNA fragments from GeneArt (Thermo Fisher Scientific) and cloned them into the phCMV3 vector (Genlantis). To keep the soluble spike proteins in a stable trimeric prefusion state, the following changes in the constructs were made: double proline substitutions (2P) were introduced in the S2 subunit; the furin cleavage sites (in SARS-CoV-2 residues 682–685 and in SARS-CoV-1 residues 664–667) were replaced by a GSAS linker; the trimerization motif T4 fibritin was incorporated at the C terminus of the spike proteins. To purify and biotinylate the spike proteins, the HRV-3C protease cleavage site, 6× His-Tag and AviTag spaced by GS linkers were added to the C terminus after the trimerization motif. To produce truncated proteins of SARS-CoV-1 and SARS-CoV-2 spike, PCR amplifications of the gene fragments encoding SARS-CoV-1 RBD (residues 307–513), SARS-CoV-2 N-terminal domain (NTD) (residues 1–290), RBD (residues 320–527), RBD-SD1 (residues 320–591) and RBD-SD1-2 (residues 320–681) subdomains were carried out using the SARS-CoV-1 and SARS-CoV-2 plasmids as templates. To generate pseudoviruses of nonhuman sarbecoviruses, the DNA fragments encoding the spikes of the sarbecoviruses without the endoplasmic reticulum retrieval signal were codon-optimized and synthesized at GeneArt. The spike-encoding genes of Pang17 (residues 1–1,249, GenBank ID: QIA48632.1), WIV1 (residues 1–1,238, GenBank ID: KF367457) and SHC014 (residues 1–1,238, GenBank ID: AGZ48806.1) were constructed into the phCMV3 vector (Genlantis) using the Gibson assembly (catalog no. E2621L; New England Biolabs) according to the manufacturer's instructions. To express the monomeric RBDs of sarbecovirus clades (clades 1a, 1b, 2 and 3), the conserved region aligning to the SARS-CoV-2 RBD (residues 320–527) were constructed into the phCMV3 vector with 6× His-Tag and AviTag spaced by GS linkers on C terminus. The sarbecovirus RBD genes encoding RaTG13 (residues 320–527, GenBank ID: QHR63300.2), Pang17 (residues 318–525, GenBank ID: QIA48632.1), WIV1 (residues 308–514, GenBank ID: KF367457), RsSHC014 (residues 308–514, GenBank ID: AGZ48806.1), BM-4831 (residues 311–514, GenBank ID: NC_014470.1), BtKY72 (residues 310–516, GenBank ID: KY352407), RmYN02 (residues 299–487, GISAID ID: EPI_ISL_412977), Rf1 (residues 311–499, GenBank ID: DQ412042.1), Rs4081 (residues 311–499, GenBank ID: KY417143.1) and Yun11 (residues 311–499, GenBank ID: JX993988) were synthesized at GeneArt and constructed using the Gibson assembly.

Cell lines. HEK-293F (Thermo Fisher Scientific) and Expi293F cells (Thermo Fisher Scientific) were maintained using FreeStyle 293 Expression Medium (Thermo Fisher Scientific) and Expi293 Expression Medium (Thermo Fisher Scientific), respectively. HEK-293F and Expi293F cell suspensions were maintained in a shaker at 150 r.p.m., 37 °C with 8% CO_2. Adherent HEK-293T cells (ATCC) were grown in DMEM supplemented with 10% FCS and 1% penicillin-streptomycin and maintained in an incubator at 37 °C with 8% CO_2. A stable human ACE2 (hACE2)-expressing HeLa cell line was generated using an ACE2 lentivirus protocol described previously. Briefly, the pBOB-hACE2 plasmid and lentiviral packaging plasmids (pMDL, pREV and pVSV-G (plasmid nos. 12251, 12253, 8454; Addgene) were cotransfected into HEK-293T cells using the Lipofectamine 2000 reagent (catalog no. 11668019; Thermo Fisher Scientific).

Transfection for protein expression. To express mAbs, the HC and LC gene segments that were cloned into corresponding expression vectors were transfected into Expi293 cells (Thermo Fisher Scientific) (2–3 million cells ml^{-1}) using the FectoPRO reagent (catalog no. 116-040; Polyplus) for a final expression volume of 2, 4 or 50 ml. After approximately 24 h, sodium valproic acid and glucose were added to the cells at a final concentration of 300 mM each. Cells were allowed to incubate for an additional 4 d to allow for mAb expression. To express spike proteins, RBDs and NTDs, cloned plasmids (350 µg) were transfected into HEK-293F cells (1 million cells ml^{-1}) using the transfectagro reagent (Corning) and 40,000 molecular weight polyethylenimine (PEI) (1 mg ml^{-1}) in a final expression volume of 1 l as described previously. Briefly, plasmid and transfection reagents were combined and filtered before PEI was added. The combined transfection solution was allowed to incubate at room temperature for 30 min before being gently added to cells. After 5 d, the supernatant was centrifuged and filtered.

Protein purification. For mAb purification, a 1:1 solution of Protein A Sepharose (GE Healthcare) and Protein G Sepharose (GE Healthcare) was added to the Expi293 supernatant for 2 h at room temperature or overnight at 4 °C. The solution was then loaded into an Econo-Pac column (catalog no. 7321010; Bio-Rad Laboratories) and washed with 1 column volume of PBS; mAbs were eluted with 0.2 M citric acid (pH 2.67). The elution was collected into a tube containing 2 M Tris base. Buffer was exchanged with PBS using 30 K Amicon centrifugal filters (catalog no. UFC903008; Merck Millipore). His-tagged proteins were purified using HisPur Ni-NTA Resin (Thermo Fisher Scientific). Resin-bound proteins were washed (25 mM imidazole, pH 7.4) and slowly eluted (250 mM imidazole, pH 7.4) with 25 ml elution buffer. Eluted proteins were buffer-exchanged with PBS and further purified using size-exclusion chromatography with Superdex 200 (GE Healthcare).

ELISA. ELISA was performed on 96-well half-area microplates (Thermo Fisher Scientific) as described previously[66]. The plate was coated with 2 µg ml^{-1} mouse anti-His antibody (catalog no. MA1-21315-1MG; Thermo Fisher Scientific) overnight at 4 °C. The following day, plates were washed 3 times with PBST (PBS + 0.05% Tween 20) and incubated for 1 h with blocking buffer (3% BSA). After removal of the blocking buffer, plates were treated with His-tagged proteins (5 µg ml^{-1} in PBST + 1% BSA) for 1.5 h at room temperature. Plates were washed and serum was added at threefold dilutions (beginning at 1:30) and allowed to incubate for 1.5 h. After washing, secondary antibody (AffiniPure goat anti-human IgG Fc fragment-specific, catalog no. 109-055-008; Jackson ImmunoResearch) was added at 1:1,000 for an additional 1 h. Secondary antibody was washed out and staining substrate (alkaline phosphatase substrate p-nitrophenyl phosphate tablets; Sigma-Aldrich) was added. Absorbance at 405 nm was measured after 8, 20 and 30 min using the VersaMax microplate reader (Molecular Devices) and analyzed with SoftMax v.5.4 (Molecular Devices).

Protein biotinylation. To randomly biotinylate the proteins described in this article, we used an EZ-Link NHS-PEG Solid-Phase Biotinylation Kit (catalog no. 21440; Thermo Scientific Scientific). To dissolve the reagents supplied in the kit for stock solutions, 10 µl dimethylsulfoxide was added into each tube. To make a working solution, 1 µl stock solution was diluted by 170 µl water freshly before use. To concentrate the proteins before biotinylation, appropriately sized filter Amicon tubes were used. Proteins were adjusted to 7–9 mg ml^{-1} in PBS. For each 30 µl of aliquoted protein, 3 µl of working solution was added and mixed thoroughly following by a 3-h incubation on ice. To stop the reaction and remove the free NHS-PEG4-Biotin, the protein solution was buffer-exchanged into PBS using Amicon tubes. All proteins were evaluated by BLI after biotinylation.

BirA biotinylation of proteins for B cell sorting. For B cell sorting, the spike probes with the His and AviTag at the C terminus were biotinylated by the intracellular biotinylating reaction during the transfection step. To biotinylate the recombinant Avi-tagged spike probes, the BirA biotin-protein ligase encoding the plasmid was cotransfected with the spike probe-AviTag-encoding plasmids in the FreeStyle 293F cell. Then, 150 µg BirA plasmid and 300 µg spike probe plasmids were transfected with PEI reagent as described above. The spike probes were purified with HisPur Ni-NTA Resin as described above. After purification, biotinylated proteins were evaluated by BLI.

BLI. Binding assays were performed on an Octet RED384 instrument using Anti-Human IgG Fc Capture biosensors (ForteBio). All samples were diluted in Octet buffer (PBS with 0.1% Tween 20) for a final concertation of 10 µg ml^{-1} for mAbs and 200 nM for viral proteins. To screen the supernatant mAb binding, 125 µl of expression supernatant was used. For the binding assays, antibodies were captured for 60 s and transferred to buffer for an additional 60 s. Captured antibodies were dipped into viral proteins for 120 s to obtain an association signal. For dissociation, biosensors were moved to Octet buffer only for an additional 240 s for the dissociation step. The data generated were analyzed using the ForteBio Data Analysis software (version 12) for correction; the kinetic curves were fitted to a 1:1 binding mode. Note that the IgG:spike protomer binding can be a mixed population of 2:1 and 1:1, such that 'apparent affinity' dissociation constants (Kd_{app}) are shown to reflect the binding affinity between IgGs and the spike trimers tested.

Isolation of mAbs. To isolate antigen-specific memory B cells, we used SARS-CoV-1 and SARS-CoV-2 spike proteins as probes to perform single-cell sorting in a 96-well format. PBMCs from postinfection vaccinated human donors were stained with fluorophore-labeled antibodies and spike proteins. To generate spike probes, streptavidin Alexa Fluor 647 (AF647) (catalog no. S32357; Thermo Fisher Scientific) was coupled to BirA biotinylated SARS-CoV-1 spike. Streptavidin Alexa Fluor 488 (AF488) (catalog no. S32354; Thermo Fisher Scientific) and streptavidin-Brilliant Violet 421 (BV421) (catalog no. 563259; BD Biosciences) were coupled to BirA biotinylated SARS-CoV-2 spike separately. The conjugation reaction was carried freshly before use with spike protein versus

streptavidin-fluorophores at a 2:1 or 4:1 molecular ratio. After 30-min incubation at room temperature, the conjugated spike proteins were stored on ice or at 4 °C for up to 1 week. To prepare PBMCs, frozen PBMCs were thawed in 10 ml recovery medium (Roswell Park Memorial Institute 1640 medium containing 50% FCS) immediately before staining. Cells were washed with 10 ml fluorescence-activated cell sorting (FACS) buffer (PBS, 2% FCS, 2 mM EDTA) and each 10 million cells were resuspended in 100 µl of FACS buffer. To isolate SARS-CoV-1 and SARS-CoV-2 cross-reactive IgG$^+$ B cells, PBMCs were stained for CD3 (APC Cy7, catalog no. 557757; BD Biosciences), CD4 (APC Cy7, catalog no. 317418; BioLegend), CD8 (APC Cy7, catalog no. 557760; BD Biosciences), CD14 (APC-H7, clone M5E2, catalog no. 561384; BD Biosciences), CD19 (PerCP-Cyanine5.5, clone HIB19, catalog no. 302230; BioLegend), CD20 (PerCP-Cyanine 5.5, clone 2H7, catalog no. 302326; BioLegend), IgG (BV786, clone G18-145, catalog no. 564230; BD Biosciences) and IgM (PE, clone MHM-88, catalog no. 314508; BioLegend). All antibodies were used in a 1:20 dilution. Antibodies were incubated with PBMCs on ice for 15 min. After the 15-min staining, 0.5 µg SARS-CoV-1-S-AF647, 1.6 µg SARS-CoV-2-S-AF488 and 1.6 µg SARS-CoV-2-S-BV421 were added to the PBMC solution and incubated on ice. After another 30-min incubation, FVS510 LIVE/DEAD stain (catalog no. L34966; Thermo Fisher Scientific) diluted 1:1,000 with FACS buffer was added to the PBMC solution for 15 min. Subsequently, cells were washed with 10 ml ice-cold FACS buffer. Each 10 million cells were resuspended with 500 µl FACS buffer and then filtered through 70-µm nylon mesh FACS tube caps (catalog no. 08-771-23; Thermo Fisher Scientific). A BD FACSMelody sorter (BRV 9 Color Plate 4way) was used for the single-cell sorting process. To isolate cross-reactive B cells, the gating strategy was set as follows: lymphocytes (side scatter area versus forward scatter area (FSC-A)) and singlets (foward scatter height versus FSC-A) were gated first; then live cells were selected by FVS510 LIVE/DEAD negative gating. B cells were identified as CD19$^+$CD20$^+$CD3$^-$CD4$^-$CD8$^-$CD14$^-$IgM-IgG$^+$ live singlets. Cross-reactive spike protein-specific B cells were sequentially selected for SARS-CoV-2-S-BV421/SARS-CoV-2-S-AF488 double positivity and SARS-CoV-1-S-AF647/SARS-CoV-2-S-AF488 double positivity. Single cells were sorted into 96-well plates on a cooling platform. To prevent degradation of mRNA, plates were moved onto dry ice immediately after sorting. Reverse transcription was done right after. SuperScript IV Reverse Transcriptase (Thermo Fisher Scientific), deoxyribonucleotide triphosphates (Thermo Fisher Scientific), random hexamers (GeneLink), Ig gene-specific primers, dithiothreitol, RNaseOUT (Thermo Fisher Scientific) and IGEPAL (Sigma-Aldrich) were used in the PCR reaction with reverse transcription as described previously[82,83]. To amplify IgG HC and LC variable regions, two rounds of nested PCR reactions were carried out using the complementary DNAs as the template and Hot Start DNA Polymerases (Thermo Fisher Scientific) and specific primer sets described previously[82,83]. The PCR products of the HC and LC variable regions were purified with Solid Phase Reversible Immobilization beads according to the manufacturer's instructions (Beckman Coulter). Then, the purified DNA fragments were constructed into expression vectors encoding human IgG1, and Ig κ/λ constant domains, respectively. Gibson assembly was used according to the manufacturer's instructions in the construction step. To produce mAbs, the paired HCs and LCs were cotransfected into Expi293 cells.

Immunogenetics analysis. HC and LC sequences of mAbs as well as ten repertoire sequencing libraries representing the naive HC repertoires of ten donors (ERR2567178–ERR2567187) from BioProject PRJEB26509 (ref. [81]) were processed using the Diversity Analyzer tool[84]. Clonal lineages for mAbs were computed in three steps. The first step was applied to the HC sequences according to the procedures described previously[85]. Briefly, HC sequences were combined into the same clonal lineage if (1) they shared V and J germline genes, (2) their CDR H3s had the same lengths and (3) their CDR H3s shared at least 90% nucleotide identity. As the second step, the same procedure was applied to the LC sequences. Finally, each HC clonal lineage was split according to the clonal lineage assignments of the corresponding LC sequences. Phylogenetic trees derived from the HC sequences and *IGHD* gene segments of mAbs were constructed using the Clustal W2 tool (version 1.2.2; https://www.ebi.ac.uk/Tools/msa/clustalo)[86] and visualized using the Iroki tool (https://www.iroki.net)[87].

Pseudovirus production. To generate pseudoviruses, plasmids encoding the SARS-CoV-1, SARS-CoV-2 or spike proteins of other variants with the endoplasmic reticulum retrieval signal removed were cotransfected with the murine leukemia virus (MLV) Gag/Pol and MLV-cytomegalovirus (CMV)-luciferase plasmids into HEK-293T cells (ATCC). Lipofectamine 2000 was used according to the manufacturer's instructions; 48 h posttransfection, the supernatants containing pseudoviruses were collected and filtered through a 0.22-µm membrane to remove debris. Pseudoviruses were stored at −80 °C before use.

Pseudovirus entry and serum neutralization assays. To generate hACE2-expressing stable cell lines for the pseudovirus infection test, we used lentivirus to transduce the hACE2 into HeLa cells (ATCC). Stable cell lines with consistent and high hACE2 expression levels were established as HeLa-hACE2 and used in the pseudovirus neutralization assay. To calculate the neutralization efficiency of the sera or mAbs, samples were serially diluted threefold and 25 µl of each dilution was incubated with 25 µl of pseudovirus at 37 °C for 1 h in 96 half-area well plates (catalog no. 3688; Corning). Just before the end of the incubation, HeLa-hACE2 cells were suspended with culture medium at a concentration of 2×10^5 ml^{-1}. DEAE-dextran (catalog no. 93556-1G; Sigma-Aldrich) was added to the cell solutions at 20 µg ml^{-1}. Then, 50 µl of the cell solution was distributed into each well. Plates were incubated at 37 °C for 2 d and neutralization efficiency was calculated by measuring the luciferase levels in the HeLa-hACE2 cells. After removal of the supernatant, the HeLa-hACE2 cells were lysed using luciferase lysis buffer (25 mM Gly-Gly, pH 7.8, 15 mM $MgSO_4$, 4 mM EGTA, 1% Triton X-100) at room temperature for 10–20 min. After adding Bright-Glo (catalog no. PRE2620; Promega Corporation) to each well, luciferase activity was inspected with a luminometer. Each experiment was carried out with duplicate samples and repeated independently at least twice. Percentage of neutralization was calculated according to the following equation:

$$\text{Percentage neutralization} = 100 \times \left(1 - \frac{(\text{RLU of sample}) - (\text{Average RLU of CC})}{(\text{Average RLU of VC}) - (\text{Average RLU of CC})}\right)$$

The neutralization percentage was calculated and plots against antibody concentrations or serum dilution ratios were made in Prism 8 (Graph Pad Software). The curves were fitted by nonlinear regression and the 50% pseudovirus neutralizing (IC_{50}) or binding (minimal infective dose (ID_{50})) antibody titer was calculated.

Neutralization assay of replication-competent sarbecoviruses. VERO C1008 cells (ATCC) were seeded at 2×10^4 cells per well in a black-well, black-wall, tissue culture-treated, 96-well plate (catalog no. 3916; Corning) 24 h before the assay. MAbs were diluted in MEM supplemented with 5% FCS and 1% penicillin-streptomycin medium to obtain an 8-point, threefold dilution curve with starting concentration at 20 µg ml^{-1}. Eight hundred plaque-forming units (PFUs) of SARS1-nLuc, SARS2-D614G-nLuc and SHC014-nLuc replication-competent viruses were mixed with mAbs at a 1:1 ratio and incubated at 37 °C for 1 h. One hundred microliters of virus and mAb mix was added to each well and incubated at 37 °C + 5% CO_2 for 20–22 h. Luciferase activity was measured with the Nano-Glo Luciferase Assay System (catalog no. N1130; Promega Corporation) according to the manufacturer's protocol using a GloMax luminometer (Promega Corporation). Percentage inhibition and IC_{50} were calculated as in the pseudovirus neutralization assay described above. All experiments were performed in duplicate and repeated independently three times. All the live virus experiments were performed under biosafety level 3 conditions at negative pressure, by operators in Tyvek suits wearing personal powered air purifying respirators.

Competition BLI. To determine the binding epitopes of the isolated mAbs compared with known human SARS-CoV-2 mAbs, we did in-tandem epitope binning experiments using the Octet RED384 system; 200 nM of randomly biotinylated SARS-CoV-2 spike or RBD protein antigen was captured using streptavidin biosensors (catalog no. 18-5019; Sartorius). The biosensor was loaded with antigen for 5 min and then moved into the saturating mAbs at a concentration of 100 µg ml^{-1} for 10 min. The biosensors were then moved into the bnAb solution for 5 min to measure binding in the presence of saturating antibodies. As control, biosensors loaded with antigen were directly moved into the bnAb solution. The percentage (%) inhibition in binding was calculated with the following formula: (percentage (%) binding inhibition = 1 − (bnAb binding response in the presence of the competitor antibody/binding response of the corresponding control bnAb without the competitor antibody)).

Fab production. To generate the Fab from the IgG, a stop codon was inserted in the HC constant region at KSCDK. The truncated HCs were cotransfected with the corresponding LCs in Expi293F cells to produce the Fabs. The supernatants were collected 4 days posttransfection. Fabs were purified with CaptureSelect CH1-XL MiniChrom Columns (catalog no. 5943462005; Thermo Fisher Scientific). Supernatants were loaded onto columns using an Econo Gradient Pump (catalog no. 7319001; Bio-Rad Laboratories). After a wash with 1× PBS, Fabs were eluted with 25 ml of 50 mM acetate (pH 4.0) and neutralized with 2 M Tris base. The eluate was buffer-exchanged with 1× PBS in 10,000 Amicon tubes (catalog no. UFC901008; Merck Millipore) and filtered with a 0.22-µm spin filter.

Negative stain electron microscopy. Spike protein was complexed with Fab at three times molar excess per trimer and incubated at room temperature for 30 min. Complexes were diluted to 0.03 mg ml^{-1} in 1× Tris-buffered saline and 3 µl applied to a 400mesh Cu grid, blotted with filter paper, and stained with 2% uranyl formate. Micrographs were collected on a Tecnai Spirit microscope (FEI Tecnai) operating at 120 kV with an FEI Eagle charge-coupled device (4×4k) camera at ×52,000 magnification using the Leginon automated image collection software (version 3.5)[88]. Particles were picked using Dog Picker (v1.0)[89] and data was processed using RELION 3.0 (ref. [90]). Map segmentation was performed in UCSF Chimera[91].

In vivo infections. All mouse experiments were performed at the University of North Carolina, National Institutes of Health/Public Health Service Animal Welfare Assurance no. D16-00256 (A3410-01), under approved Institutional Animal Care and Use Committee protocols. All animal manipulation and virus work was performed in a class 2A biological safety cabinet. Twelve-month-old female BALB/c mice (strain 047) were purchased from Envigo. Mice were housed in individually ventilated Sealsafe cages, provided with food and water ad libitum and allowed to acclimate at least 7 d before experimental use. Twelve hours before infection, mice were injected intraperitoneally with 300 µg of antibody. Immediately before infection, mice were anesthetized by intraperitoneal injection of ketamine and xylazine and weighed. Virus was diluted in 50 µl of sterile PBS and administered intranasally. Mice were weighed daily and observed for signs of disease. At the designated time, mice were euthanized via isoflurane overdose, gross lung pathology was assessed and the inferior lobe was collected for virus titration. Respiratory function was measured at day 2 postinfection via Buxco whole-body plethysmography, as described by Menachery et al.[92]. No animals or data points were excluded from the analyses.

Virus titration. SARS-CoV-2 MA10, SARS-CoV-1 MA15 and chimeric SARS-CoV-1 MA15-SHC014 were grown and titered using VERO C1008 cells as described by Yount et al.[93]. Briefly, lung tissue was homogenized in 1 ml sterile PBS via MagNA Lyser (Roche), centrifuged to pellet debris, plated in 10-fold serial dilutions on VERO C1008 cells on a 6-well plate and covered with a 1:1 mixture of 1.6% agarose and medium. At two (SARS-CoV-1) or three (SARS-CoV-2) days post-plating, cells were stained with neutral red and plaques were counted.

Statistical analysis. Statistical analysis was performed using Prism 8 for Mac. Statistical comparisons between the two groups were performed using a two-tailed Mann–Whitney *U*-test. The correlation between two groups was determined by Spearman rank test. Groups of data were compared using the Kruskal–Wallis nonparametric test. Dunnett's multiple comparisons tests were also performed between experimental groups. Data were considered statistically significant at $^{*}P<0.05$, $^{**}P<0.01$, $^{***}P<0.001$ and $^{****}P<0.0001$. Data collection and analysis were not performed blind to the conditions of the experiments. We did not use any statistical methods to predetermine sample sizes for the animal studies. No data points were excluded as outliers in any of the experiments.

Reporting summary. Further information on research design is available in the Nature Research Reporting Summary linked to this article.

Data availability

All the data supporting the findings of this study are available within the paper and its supplementary information files; any remaining information can be obtained from the corresponding author upon reasonable request. Antibody sequences have been deposited in GenBank under accession nos. OM467906–OM468119. The negative stain electron microscopy (ns-EM) maps of RBD bnAb Fabs in complex with SARS-CoV-2 S-protein has been deposited to the Electron Microscopy Data Bank (EMDB) under accession IDs EMDB-26365-26375.

References

82. Tiller, T. et al. Efficient generation of monoclonal antibodies from single human B cells by single cell RT–PCR and expression vector cloning. *J. Immunol. Methods* **329**, 112–124 (2008).
83. Doria-Rose, N. A. et al. New member of the V1V2-directed CAP256-VRC26 lineage that shows increased breadth and exceptional potency. *J. Virol.* **90**, 76–91 (2015).
84. Shlemov, A. et al. Reconstructing antibody repertoires from error-prone immunosequencing reads. *J. Immunol.* **199**, 3369–3380 (2017).
85. Roskin, K. M. et al. Aberrant B cell repertoire selection associated with HIV neutralizing antibody breadth. *Nat. Immunol.* **21**, 199–209 (2020).
86. Larkin, M. A. et al. Clustal W and Clustal X version 2.0. *Bioinformatics* **23**, 2947–2948 (2007).
87. Moore, R. M., Harrison, A. O., McAllister, S. M., Polson, S. W. & Wommack, K. E. Iroki: automatic customization and visualization of phylogenetic trees. *PeerJ* **8**, e8584 (2020).
88. Suloway, C. et al. Automated molecular microscopy: the new Leginon system. *J. Struct. Biol.* **151**, 41–60 (2005).
89. Voss, N. R., Yoshioka, C. K., Radermacher, M., Potter, C. S. & Carragher, B. DoG Picker and TiltPicker: software tools to facilitate particle selection in single particle electron microscopy. *J. Struct. Biol.* **166**, 205–213 (2009).
90. Scheres, S. H. RELION: implementation of a Bayesian approach to cryo-EM structure determination. *J. Struct. Biol.* **180**, 519–530 (2012).
91. Pettersen, E. F. et al. UCSF Chimera—a visualization system for exploratory research and analysis. *J. Comput. Chem.* **25**, 1605–1612 (2004).
92. Menachery, V. D., Gralinski, L. E., Baric, R. S. & Ferris, M. T. New metrics for evaluating viral respiratory pathogenesis. *PLoS ONE* **10**, e0131451 (2015).
93. Yount, B. et al. Severe acute respiratory syndrome coronavirus group-specific open reading frames encode nonessential functions for replication in cell cultures and mice. *J. Virol.* **79**, 14909–14922 (2005).

Acknowledgements

We thank all the human cohort participants for donating samples. This work was supported by National Institutes of Health (NIH) CHAVD UM1 AI44462 (D.R.B.), the International AIDS Vaccine Initiative Neutralizing Antibody Center, Bill and Melinda Gates Foundation INV-004923 (I.A.W., A.B.W. and D.R.B.), Translational Virology Core of the San Diego Center for AIDS research grant NIH AI036214 (D.M.S.), NIH 5T32AI007384 (S.A.R.), NIH AI149644 and AI157155 (R.S.B), NIH R21 AI145372 (L.E.G.) and the John and Mary Tu Foundation and the James B. Pendleton Charitable Trust (D.M.S. and D.R.B.). L.V.T. is supported by the Pfizer NCBiotech Distinguished Postdoctoral Fellowship in Gene Therapy. D.R.M. is currently supported by a Burroughs Wellcome Fund Postdoctoral Enrichment Program Award and a Hanna H. Gray Fellowship from the Howard Hughes Medical Institute.

Author contributions

W.H., R.M., G.S., K.D., D.R.B. and R.A. conceived and designed the study. N.B., M.P., E.G., S.A.R., D.M.S. and T.F.R. recruited the donors and collected and processed the plasma and PBMC samples. W.H., R.M., G.S., K.D., S.C., T.C., P.Y. and F.A. performed the BLI, ELISA, virus preparation, neutralization and isolation and characterization of mAbs. Y.S. performed the immunogenetic analysis of antibodies. P.Z. prepared the virus mutant plasmids. J.L.T. and R.M.V. conducted the negative stain electron microscopy studies. M.Y. and H.L. generated the antibody–antigen structural models. L.V.T. performed the live virus neutralizations assays and L.V.T., D.R.M., A.S. and L.E.G. conducted the in vivo animal protection studies. W.H., R.M., G.S., K.D., L.V.T., D.R.M., A.S., S.C., P.Y., N.B., J.L.T., R.M.V., P.Z., M.Y., H.L., F.A., M.P., E.G., I.A.W., A.B.W., T.F.R., R.S.B., L.E.G., D.R.B. and R.A. designed the experiments and/or analyzed the data. W.H., R.M., D.R.B. and R.A. wrote the paper; all authors reviewed and edited the paper.

Competing interests

W.H., R.M., G.S., K.D., T.F.R., D.R.B. and R.A. are listed as inventors on pending patent applications describing the sarbecovirus broadly neutralizing antibodies isolated in this study. A.B.W., I.A.W. and D.R.B. receive research funding from Adagio. R.S.B. and L.E.G. have ongoing collaborations with Adagio. The other authors declare no competing interests.

Additional information

Extended data is available for this paper at https://doi.org/10.1038/s41590-022-01222-1.

Supplementary information The online version contains supplementary material available at https://doi.org/10.1038/s41590-022-01222-1.

Correspondence and requests for materials should be addressed to Ralph S. Baric, Lisa E. Gralinski, Dennis R. Burton or Raiees Andrabi.

Peer review information *Nature Immunology* thanks the anonymous reviewers for their contribution to the peer review of this work. Peer reviewer reports are available. N. Bernard was the primary editor on this article and managed its editorial process and peer review in collaboration with the rest of the editorial team.

Reprints and permissions information is available at www.nature.com/reprints.

a

	Strain	CC12	CC27	CC34	CC35	CC36	CC38
COVID-19	SARS-CoV-2	639	170	269	1340	586	230
	B.1.1.7	1413	150	219	1824	758	3724
	B.1.351	<60	64	<60	85	<60	<60
	P.1	<60	378	<60	<60	<60	<60
	B1.617.2	119	685	501	1822	320	554
	B.1.1.529	<60	<60	<60	<60	<60	<60
	Pang17	79	<60	<60	149	89	<60
	SARS-CoV-1	<60	<60	<60	<60	<60	<60
	WIV1	101	<60	<60	<60	<60	<60

	Strain	CC102	CC103	CC104	CC105	CC106	CC107	CC108	CC109	CC110	CC111
2X vaccinated	SARS-CoV-2	185	544	263	870	789	303	486	288	163	76
	B.1.1.7	<60	326	132	720	422	117	369	211	<60	<60
	B.1.351	<60	95	<60	168	115	<60	67	<60	<60	<60
	P.1	<60	<60	123	<60	107	<60	<60	<60	<60	<60
	B1.617.2	<60	72	162	159	93	<60	97	<60	<60	<60
	B.1.1.529	<60	<60	<60	<60	<60	<60	<60	<60	<60	<60
	Pang17	<60	70	<60	515	427	411	283	<60	<60	<60
	SARS-CoV-1	<60	<60	<60	<60	<60	<60	<60	<60	<60	<60
	WIV1	<60	148	<60	228	123	<60	111	<60	<60	<60

	Strain	CC9	CC24	CC25	CC26	CC42	CC62	CC67	CC68	CC74	CC78	CC80	CC84	CC92	CC95	CC99
infected (before vaccination)	SARS-CoV2	68	<60	1204	<60	<60	<60	<60	<60	349	<60	<60	<60	169	<60	<60
	B.1.1.7	<60	<60	903	<60	<60	<60	<60	<60	174	<60	<60	<60	83	<60	<60
	B.1.351	<60	<60	149	<60	<60	<60	<60	<60	130	<60	<60	<60	<60	<60	<60
	P.1	<60	<60	<60	<60	<60	<60	<60	<60	<60	<60	<60	<60	<60	<60	<60
	B1.617.2	<60	<60	357	<60	<60	<60	<60	<60	111	<60	<60	<60	190	<60	<60
	B.1.1.529	<60	<60	<60	<60	<60	<60	<60	<60	<60	<60	<60	<60	<60	<60	<60
	Pang17	<60	<60	<60	<60	<60	<60	<60	<60	<60	<60	<60	<60	<60	<60	<60
	SARS-CoV-1	<60	<60	<60	<60	<60	<60	<60	<60	<60	<60	<60	<60	<60	<60	<60
	WIV1	<60	<60	<60	<60	<60	<60	<60	<60	<60	<60	<60	<60	<60	<60	<60

	Strain	CC9	CC24	CC25	CC26	CC42	CC62	CC67	CC68	CC74	CC78	CC80	CC84	CC92	CC95	CC99
infected + vaccinated	SARS-CoV2	1923	244	1097	3815	62	3140	617	1488	1238	804	296	5770	1423	1235	243
	B.1.1.7	904	361	1172	1513	<60	2695	735	668	887	1545	912	2267	1840	1185	129
	B.1.351	758	156	950	842	<60	2512	843	1398	1013	1884	174	3312	3546	1997	223
	P.1	755	193	1426	657	<60	1611	529	364	566	832	<60	1167	1224	919	<60
	B1.617.2	1364	695	1972	935	<60	3193	1294	2352	702	1308	394	4908	2191	1154	149
	B.1.1.529	337	<60	621	526	<60	2081	286	524	420	702	<60	1452	864	726	<60
	Pang17	<60	76	923	362	<60	1235	729	1424	512	282	169	1160	1363	615	<60
	SARS-CoV-1	87	<60	229	110	<60	<60	<60	124	73	<60	<60	1758	<60	111	<60
	WIV1	228	336	433	290	<60	391	232	92	81	410	219	2233	672	512	82

b Gating strategy for antigen specific B cell profiling

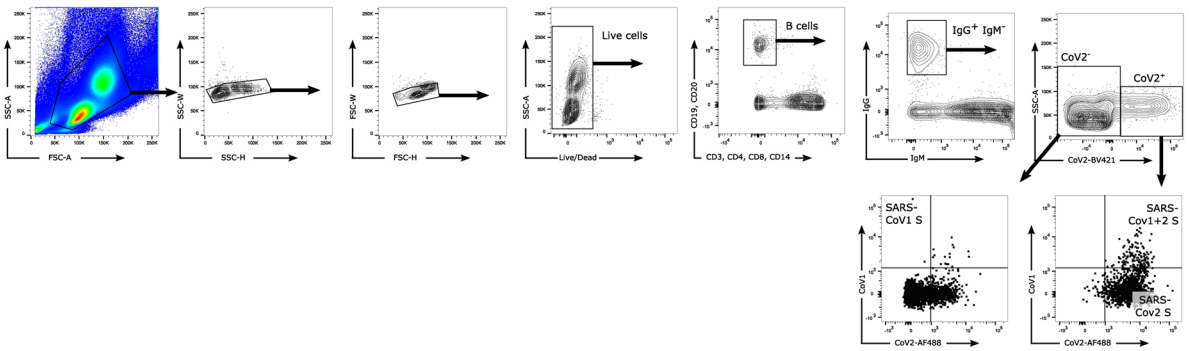

c Gating strategy for antigen specific single B cell isolation

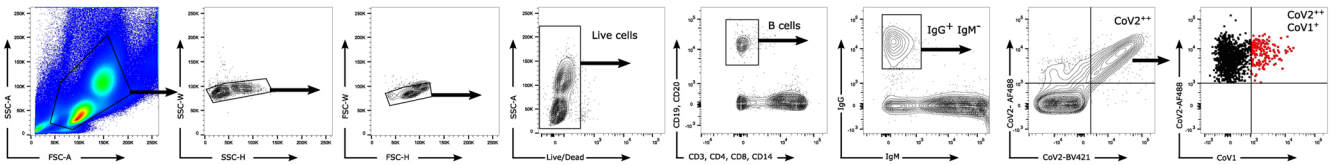

Extended Data Fig. 1 | Serum neutralization and flow cytometry B cell profiling and sorting strategies. a. Neutralization by sera from COVID-19, 2 x mRNA-spike-vaccinated and SARS-CoV-2 recovered/mRNA vaccinated donors with pseudotyped SARS-CoV-2, SARS-CoV-2 variants of concern [B.1.1.7 (Alpha), B.1.351 (Beta), P.1 (Gamma), B.1.617.2 (Delta) and B.1.1.529 (Omicron)], as well as other sarbecoviruses (Pang17, SARS-CoV-1, and WIV1). ID_{50} neutralization titers are shown. Prior to vaccination, the sera from infected-vaccinated donors were tested for neutralization and the ID_{50} neutralization titers are shown for comparison. **b**. Gating strategy for analysis of IgG^+ B cell populations that bind SARS-CoV-1 S-protein only ($CD19^+CD20^+CD3^-CD4^-CD8^-CD14^-IgM^-IgG^+CoV2BV421^-CoV2AF488^-CoV1^+$), SARS-CoV-2 S-protein only ($CD19^+CD20^+CD3^-CD4^-CD8^-CD14^-IgM^-IgG^+$ $CoV2BV421^+CoV2AF488^+CoV1^-$), or both SARS-CoV-1 and SARS-CoV-2 S-proteins ($CD19^+CD20^+CD3^-CD4^-CD8^-CD14^-IgM^-IgG^+CoV2BV421^+CoV2AF488^+CoV1^+$). **c**. Gating strategy used to isolate single cross-reactive IgG^+ B cells (indicated in red).

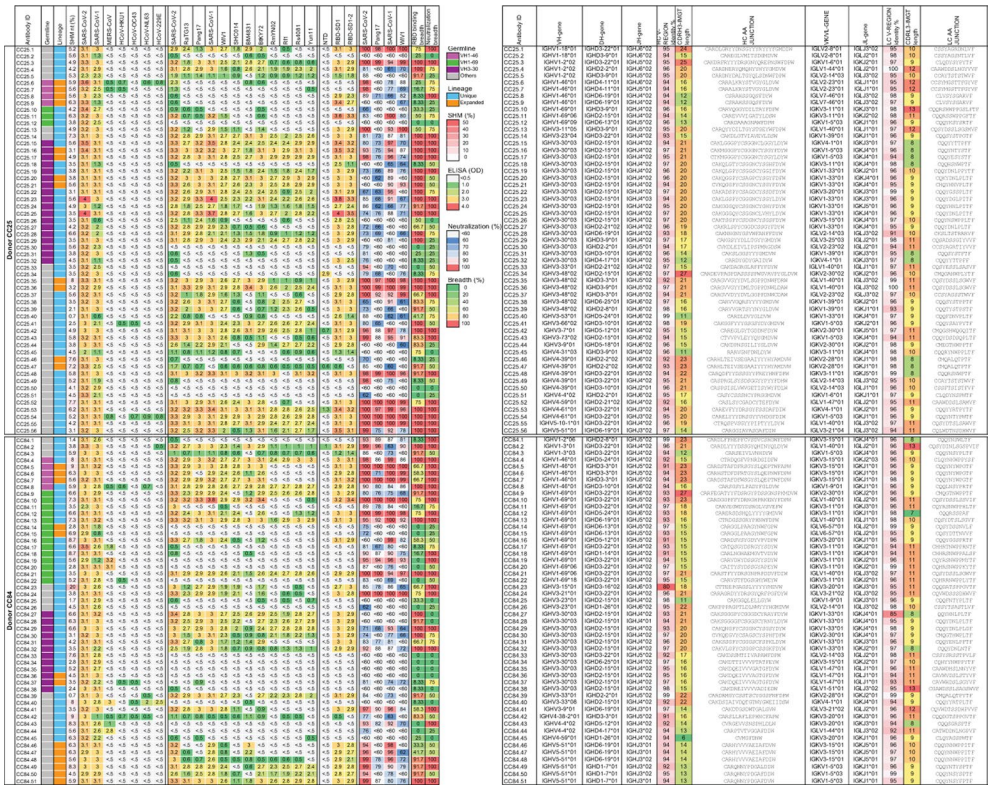

Extended Data Fig. 2 | Binding, neutralization and immunogenetics information of isolated mAbs. A total of 107 mAbs from two SARS-CoV-2 recovered-vaccinated donors CC25 (n = 56 mAbs) and CC84 (n = 51 mAbs) were isolated by single B cell sorting using SARS-CoV-1 and SARS-CoV-2 S-proteins as baits. MAbs were expressed and tested for antigen binding, pseudovirus neutralization, and analyzed for immunogenetic properties. Germline, lineage, somatic hypermutation (SHM), ELISA binding to S-proteins and RBDs, neutralization of ACE2-utilizing sarbecoviruses and breadth are colored according to the key. Paired gene information, including heavy chain CDRH3 and light chain CDRL3 sequences are represented for each mAb.

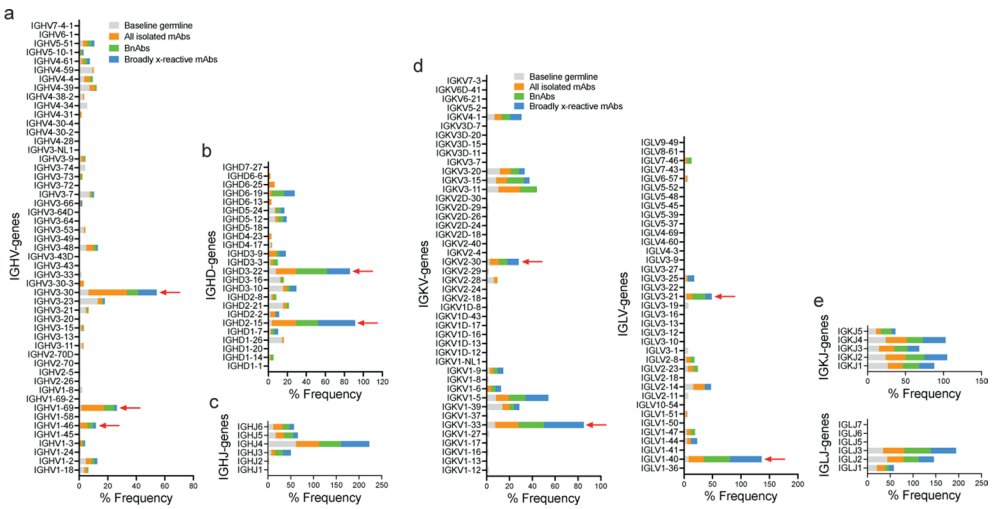

Extended Data Fig. 3 | Immunoglobulin heavy and light chain germline gene enrichments in isolated mAbs compared to a reference human germline database. Baseline germline frequencies of heavy chain genes (IGHV (**a**), IGHD (**b**) and IGHJ (**c**) genes) and light chain genes (IGKV and IGLV (**d**), IGKJ and IGLJ (**e**) genes) are shown in grey, and mAb, bnAbs and cross-reactive mAbs in a-e panels are colored according to the key in (**a** and **d**). Arrows indicate gene enrichments compared to human baseline germline frequencies. The gene usage enrichments in panels a-e are shown for all unique clone mAbs isolated from CC25 and CC84 donors. Data are shown as bar plots.

a

	SARS-CoV-2 RBD				SARS-CoV-2 S			
Antibody ID	Response (nm)	KD (M)	kon (1/Ms)	koff (1/s)	Response (nm)	KD^{App} (M)	kon (1/Ms)	koff (1/s)
CC25.1	0.4478	4.47E-10	8.27E+05	3.70E-04	0.5501	6.72E-10	4.11E+05	2.76E-04
CC25.2	-0.0007	ND	ND	ND	0.5598	7.87E-09	1.74E+05	1.37E-03
CC25.3	0.3933	3.45E-10	9.75E+05	3.36E-04	0.4959	6.38E-10	5.03E+05	3.21E-04
CC84.1	2.2865	<1.0E-12	1.99E+145	1.15E-05	0.4201	1.82E-08	8.29E+04	1.51E-03
CC84.2	2.9659	2.24E-11	6.55E+06	1.47E-04	0.6883	3.91E-09	2.71E+05	1.06E-03
CC84.3	1.9443	<1.0E-12	8.69E+109	2.81E-06	0.5503	1.47E-09	1.38E+05	2.03E-04
CC25.6	0.0136	ND	ND	ND	0.1966	5.62E-09	4.17E+05	2.34E-03
CC25.8	-0.0005	ND	ND	ND	0.6293	3.30E-10	3.24E+05	1.07E-04
CC84.4	2.4486	<1.0E-12	5.83E+06	<1.0E-07	0.699	4.54E-10	3.38E+05	1.53E-04
CC84.5	0.5613	2.95E-10	4.17E+05	1.23E-04	0.6226	6.88E-10	2.16E+05	1.49E-04
CC84.8	2.8819	<1.0E-12	5.25E+06	<1.0E-07	0.6547	7.69E-10	1.81E+05	1.39E-04
CC25.10	0.0014	ND	ND	ND	0.3418	3.52E-08	1.50E+05	5.26E-03
CC84.9	1.4974	1.48E-11	6.76E+06	1.00E-04	0.3896	7.09E-10	5.70E+05	4.04E-04
CC84.10	2.735	<1.0E-12	5.93E+06	<1.0E-07	0.7041	4.04E-10	4.05E+05	1.64E-04
CC84.12	2.0816	5.97E-12	7.28E+06	4.35E-05	0.5292	1.29E-10	5.72E+05	7.36E-05
CC84.13	3.1209	<1.0E-12	5.58E+06	<1.0E-07	0.6993	7.27E-10	2.07E+05	1.50E-04
CC84.15	1.4561	<1.0E-12	2.48E+07	<1.0E-07	0.1228	8.56E-08	1.61E+05	1.38E-02
CC84.16	0.2515	2.48E-10	1.05E+06	2.60E-04	0.3191	1.19E-10	5.70E+05	6.78E-05
CC84.17	2.0596	<1.0E-12	3.37E+08	3.69E-05	0.4423	5.16E-09	8.88E+04	4.58E-04
CC84.18	1.4043	<1.0E-12	1.86E+119	5.45E-05	0.3928	3.32E-09	1.77E+05	5.87E-04
CC84.19	1.2016	<1.0E-12	2.43E+07	<1.0E-07	0.3511	2.09E-09	1.70E+05	3.53E-04
CC25.11	0.4482	1.70E-10	4.27E+05	7.27E-05	0.5591	6.89E-10	2.43E+05	1.68E-04
CC84.20	1.3601	<1.0E-12	2.74E+07	<1.0E-07	0.4068	1.55E-09	1.73E+05	2.68E-04
CC84.21	0.3711	2.58E-10	8.94E+05	2.30E-04	0.479	5.04E-10	4.66E+05	2.35E-04
CC84.22	1.9921	<1.0E-12	4.56E+86	7.56E-05	0.4789	4.75E-09	1.09E+05	5.16E-04
CC25.13	0.485	1.88E-09	7.47E+05	1.40E-03	0.5717	3.69E-09	4.23E+05	1.56E-03
CC84.24	2.3965	1.03E-11	6.59E+06	6.78E-05	0.5723	1.02E-09	4.34E+05	4.43E-04
CC84.25	-0.0077	ND	ND	ND	0.4495	4.92E-09	7.98E+04	3.93E-04
CC25.14	0.6175	<1.0E-12	6.82E+05	<1.0E-07	0.6833	<1.0E-12	2.47E+05	<1.0E-07
CC25.15	0.6151	2.10E-10	6.61E+05	1.39E-04	0.7784	2.10E-10	3.50E+05	7.35E-05
CC25.17	0.4634	2.32E-11	8.83E+05	2.05E-05	0.5938	9.50E-11	5.12E+05	4.87E-05
CC25.18	0.09	ND	ND	ND	0.4135	8.14E-08	1.48E+05	1.20E-02
CC25.19	0.5544	1.55E-10	6.92E+05	1.07E-04	0.6963	8.21E-11	3.53E+05	2.90E-05
CC25.22	0.6459	8.76E-11	5.40E+05	4.73E-05	0.8085	4.32E-10	2.90E+05	1.25E-04
CC25.23	0.5066	7.34E-12	7.95E+05	5.84E-06	0.6468	2.09E-10	4.04E+05	8.42E-05
CC25.25	0.4356	<1.0E-12	8.18E+05	<1.0E-07	0.5548	<1.0E-12	4.05E+05	<1.0E-07
CC25.26	0.3569	1.29E-08	4.43E+05	5.73E-03	0.3824	2.08E-08	2.64E+05	5.50E-03
CC25.27	0.5103	3.21E-10	7.76E+05	2.49E-04	0.6644	4.15E-10	3.50E+05	1.45E-04
CC25.29	0.4857	2.71E-10	9.86E+05	2.67E-04	0.6287	4.47E-10	4.77E+05	2.13E-04
CC25.31	-0.0128	ND	ND	ND	0.6142	1.74E-09	1.21E+05	2.11E-04
CC25.32	-0.0025	ND	ND	ND	0.7095	1.30E-10	3.08E+05	3.99E-05
CC84.27	0.6928	<1.0E-12	9.73E+06	<1.0E-07	0.11	5.00E-10	8.99E+05	4.49E-04
CC84.29	0.4862	2.46E-10	7.05E+05	1.73E-04	0.6635	4.00E-10	3.37E+05	1.35E-04
CC84.30	0.4069	1.73E-09	1.06E+06	1.84E-03	0.5411	8.13E-10	5.57E+05	4.53E-04
CC84.31	0.4088	4.83E-10	7.61E+05	3.67E-04	0.5225	7.31E-10	3.66E+05	2.68E-04
CC84.33	0.0004	ND	ND	ND	0.5334	3.92E-09	2.20E+05	8.62E-04
CC84.34	0.0053	ND	ND	ND	0.3889	4.14E-09	3.25E+05	1.34E-03
CC84.35	-0.0238	ND	ND	ND	0.3769	4.50E-08	2.59E+05	1.17E-02
CC84.37	2.291	<1.0E-12	7.21E+102	8.41E-06	0.5937	6.17E-09	1.42E+05	8.76E-04
CC84.38	-0.0066	ND	ND	ND	0.4993	4.06E-09	1.72E+05	7.00E-04
CC25.33	0.0013	ND	ND	ND	0.4718	5.21E-08	1.51E+05	7.89E-03
CC84.39	2.4288	<1.0E-12	7.19E+108	2.75E-05	0.3177	4.93E-08	1.75E+05	8.62E-03
CC84.40	1.3971	<1.0E-12	2.18E+08	5.28E-05	0.5791	2.91E-09	1.19E+05	3.46E-04
CC25.34	-0.0023	ND	ND	ND	0.5928	1.76E-09	2.92E+05	5.15E-04
CC25.36	0.5011	1.39E-10	8.52E+05	1.18E-04	0.6133	1.26E-10	4.28E+05	5.38E-05
CC25.37	0.5589	1.40E-10	8.82E+05	1.23E-04	0.6699	3.61E-10	4.80E+05	1.73E-04
CC25.38	0.471	4.00E-10	3.71E+05	1.48E-04	0.574	4.74E-10	2.57E+05	1.22E-04
CC25.39	0.4248	2.22E-10	4.97E+05	1.10E-04	0.5146	2.77E-10	3.04E+05	8.43E-05
CC25.42	0.6007	8.18E-10	3.50E+05	2.87E-04	0.7353	5.72E-10	2.46E+05	1.41E-04
CC25.43	0.5106	<1.0E-12	9.63E+05	<1.0E-07	0.6298	5.85E-11	5.13E+05	3.00E-05
CC84.41	2.0686	<1.0E-12	6.14E+06	<1.0E-07	0.4344	2.47E-10	3.48E+05	8.59E-05
CC25.47	-0.0089	ND	ND	ND	0.1456	2.07E-08	3.01E+05	6.24E-03
CC25.48	0.4464	1.47E-11	2.93E+05	4.33E-06	0.5019	<1.0E-12	1.74E+05	<1.0E-07
CC25.49	-0.0012	ND	ND	ND	0.5078	1.08E-09	1.27E+05	ND
CC25.50	-0.0054	ND	ND	ND	0.5391	2.71E-09	1.43E+05	3.87E-04
CC25.51	-0.0106	ND	ND	ND	0.5248	6.19E-10	1.29E+05	7.99E-05
CC84.43	1.8854	<1.0E-12	3.51E+07	1.17E-05	0.2591	1.06E-07	1.00E+05	1.06E-02
CC25.52	0.6164	8.26E-11	6.93E+05	5.73E-05	0.7493	1.75E-10	3.52E+05	6.15E-05
CC84.45	2.0203	<1.0E-12	3.86E+98	3.65E-05	0.476	2.60E-09	8.95E+04	2.33E-04
CC25.53	0.4263	<1.0E-12	8.18E+05	<1.0E-07	0.5208	<1.0E-12	4.38E+05	<1.0E-07
CC25.54	0.612	2.00E-10	7.69E+05	1.54E-04	0.7409	3.69E-10	4.09E+05	1.51E-04
CC25.55	0.4682	2.87E-11	8.14E+05	2.34E-05	0.592	2.01E-11	4.56E+05	9.15E-06
CC25.56	0.4196	4.14E-10	1.09E+06	4.51E-04	0.5371	8.12E-10	5.81E+05	4.72E-04
CC84.48	2.0698	4.96E-11	6.13E+06	3.04E-04	0.4623	1.22E-08	1.63E+05	1.98E-03
CC84.51	2.984	7.32E-12	6.85E+06	5.02E-05	0.76	9.36E-10	3.57E+05	3.34E-04

b

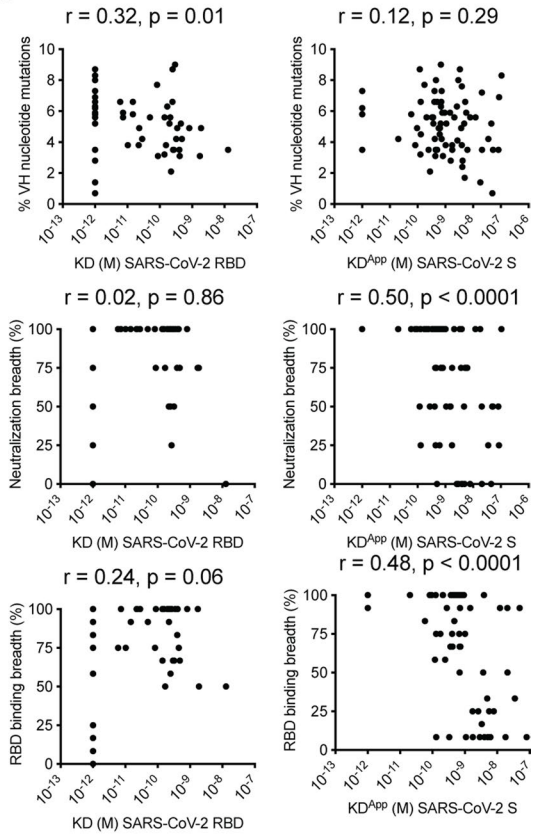

Extended Data Fig. 4 | mAb supernatant binding to SARS-CoV-2 RBD and SARS-CoV-2 S and association with SHM, binding and neutralization breadth. **a**. Supernatants from Expi293F cell-expressed mAbs were screened for BLI binding with SARS-CoV-2 RBD and SARS-CoV-2 S-protein. Binding kinetics (K_D (monomeric SARS-CoV-2 RBD) K_D^{App} (SARS-CoV-2 S-protein), k_{on} and k_{off} constants) of antibodies with human proteins are shown. Binding kinetics were obtained using the 1:1 binding kinetics fitting model on ForteBio Data Analysis software. **b**. Correlations of mAb binding (K_D or K_D^{App} (M) values) to SARS-CoV-2 RBD or S-protein with heavy chain SHMs, neutralization breadth (neutralization against 4 ACE2-using-sarbecovirus panel), and sarbecovirus RBD breadth (binding against all 12 RBDs of clades 1a, 1b, 2 and 3) are determined by nonparametric Spearman correlation two-tailed test with 95% confidence interval. The Spearman correlation coefficient (r) and p-value are indicated.

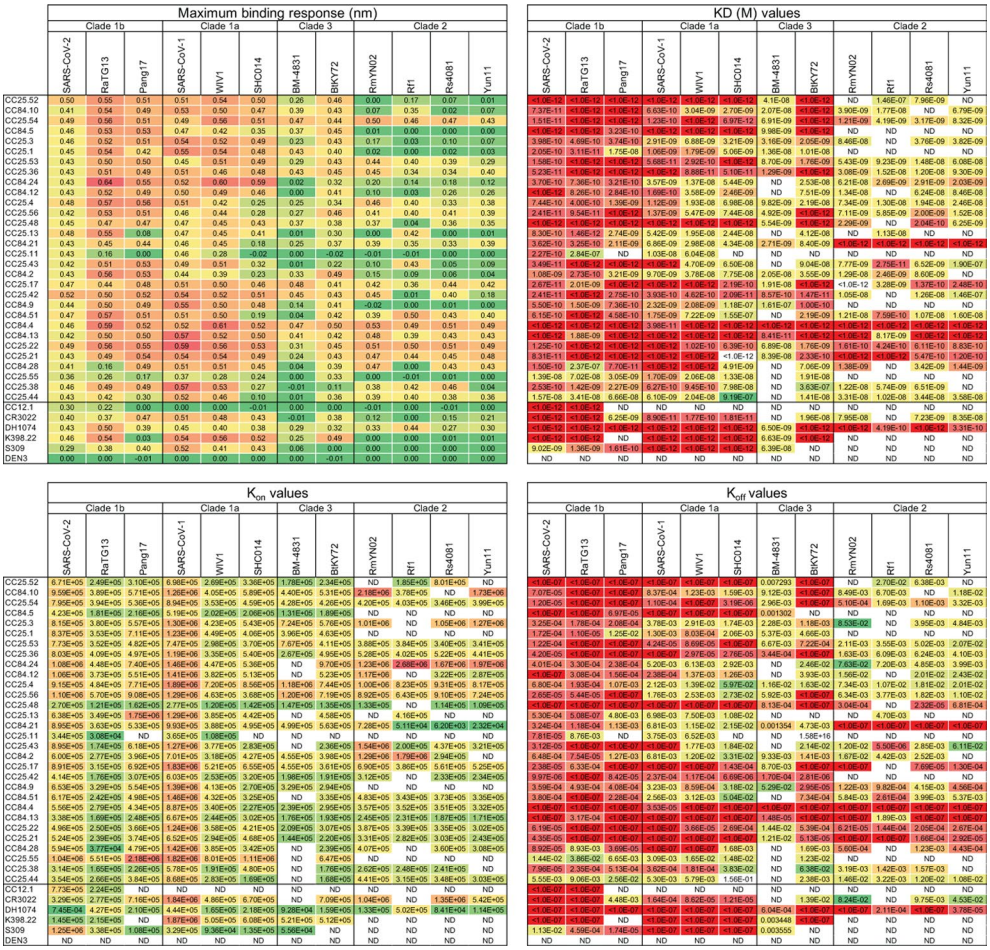

Extended Data Fig. 5 | Binding of select mAbs to RBDs from sarbecovirus clades. BLI binding kinetics of select CC25 and CC84 mAbs to monomeric RBDs derived from sarbecovirus clades: clade 1b (SARS-CoV-2, RatG13, Pang17), clade 1a (SARS-CoV-2, WIV1, SHC014), clade 3 (BM⁻4831, BtKY72) and clade 2 ((RmYN02, Rf1, Rs4081, Yun11). Binding kinetics were obtained using the 1:1 binding kinetics fitting model on ForteBio Data Analysis software and maximum binding responses, dissociations constants (K_D) and on-rate (k_{on}) and off-rate constants (k_{off}) for each antibody protein interaction are shown. K_D, k_{on} and k_{off} values were calculated only for antibody-antigen interactions where a maximum binding response of 0.05 nm was obtained.

	SARS-CoV-2					
	WT	B.1.1.7	B.1.351	P.1	B.1.617.2	B.1.1.529
CC25.52	0.12	0.07	0.11	0.09	0.08	1.10
CC84.10	0.14	0.12	0.05	0.12	0.20	0.35
CC25.54	0.13	0.13	0.18	0.07	0.15	0.69
CC84.5	0.16	0.16	0.15	0.21	0.20	>10
CC25.3	0.05	0.15	0.12	0.07	0.12	0.60
CC25.1	0.13	0.11	0.12	0.15	0.12	0.42
CC25.53	0.20	0.30	0.38	0.23	0.40	1.85
CC25.36	0.15	0.24	0.22	0.23	0.37	0.31
CC84.24	0.37	0.44	0.90	0.63	1.30	0.80
CC84.12	0.53	0.31	0.35	0.28	0.29	>10
CC25.4	0.23	0.19	0.46	0.20	0.37	1.27
CC25.56	0.51	0.74	2.74	0.49	2.33	2.18
CC25.48	1.61	1.38	0.95	1.10	1.19	>10
CC25.13	0.24	0.14	0.33	0.09	0.02	>10
CC84.21	0.19	0.22	0.10	0.10	0.16	1.43
CC25.11	2.13	0.19	0.11	1.14	1.02	>10
CC25.43	1.54	0.37	0.48	0.26	0.07	0.83
CC84.2	0.35	0.54	0.24	0.19	0.47	>10
CC25.17	4.17	0.82	1.46	0.22	0.21	2.24
CC25.42	4.87	1.49	3.59	1.25	1.14	4.95
CC12.1	0.03	0.24	>10	6.82	0.05	>10
DH1047	0.88	0.37	0.22	0.36	0.38	>10
DEN3	>10	>10	>10	>10	>10	>10

IC_{50} (μg/ml)
>10
10
1
0.1
0.01

	SARS-CoV-2					
	WT	B.1.1.7	B.1.351	P.1	B.1.617.2	B.1.1.529
CC25.52	1.0	0.6	1.0	0.8	0.7	9.4
CC84.10	1.0	0.8	0.4	0.8	1.4	2.5
CC25.54	1.0	1.0	1.5	0.6	1.2	5.4
CC84.5	1.0	1.0	0.9	1.3	1.2	61
CC25.3	1.0	3.0	2.3	1.4	2.2	11
CC25.1	1.0	0.8	0.9	1.1	0.9	3.1
CC25.53	1.0	1.5	1.9	1.2	2.0	9.1
CC25.36	1.0	1.6	1.5	1.5	2.5	2.1
CC84.24	1.0	1.2	2.4	1.7	3.5	2.2
CC84.12	1.0	0.6	0.6	0.5	0.5	19
CC25.4	1.0	0.8	2.0	0.9	1.6	5.4
CC25.56	1.0	1.5	5.4	1.0	4.6	4.3
CC25.48	1.0	0.9	0.6	0.7	0.7	6.2
CC25.13	1.0	0.6	1.4	0.4	0.1	42
CC84.21	1.0	1.1	0.5	0.5	0.8	7.4
CC25.11	1.0	0.1	0.1	0.5	0.5	4.7
CC25.43	1.0	0.2	0.3	0.2	0.0	0.5
CC84.2	1.0	1.6	0.7	0.5	1.4	29
CC25.17	1.0	0.2	0.3	0.1	0.1	0.5
CC25.42	1.0	0.3	0.7	0.3	0.2	1.0
CC12.1	1.0	7.8	333	227	1.7	333
DH1047	1.0	0.4	0.3	0.4	0.4	11
DEN3	1.0	1.0	1.0	1.0	1.0	1.0

IC_{50} Fold-change
>100
100
50
10
3

Extended Data Fig. 6 | Neutralization of RBD bnAbs against SARS-CoV-2 and major variants of concern (VOCs). IC_{50} neutralization titers of RBD bnAbs against SARS-CoV-2 (WT) and five major SARS-CoV-2 VOCs: (B.1.1.7 (Alpha), B.1.351 (Beta), P.1 (Gamma), B.1.617.2 (Delta) and B.1.1.529 (Omicron)). The IC_{50} neutralization fold-change of RBD bnAbs with SARS-CoV-2 VOCs compared to the WT virus. CC12.1, DH1047 and DEN mAbs were used as controls.

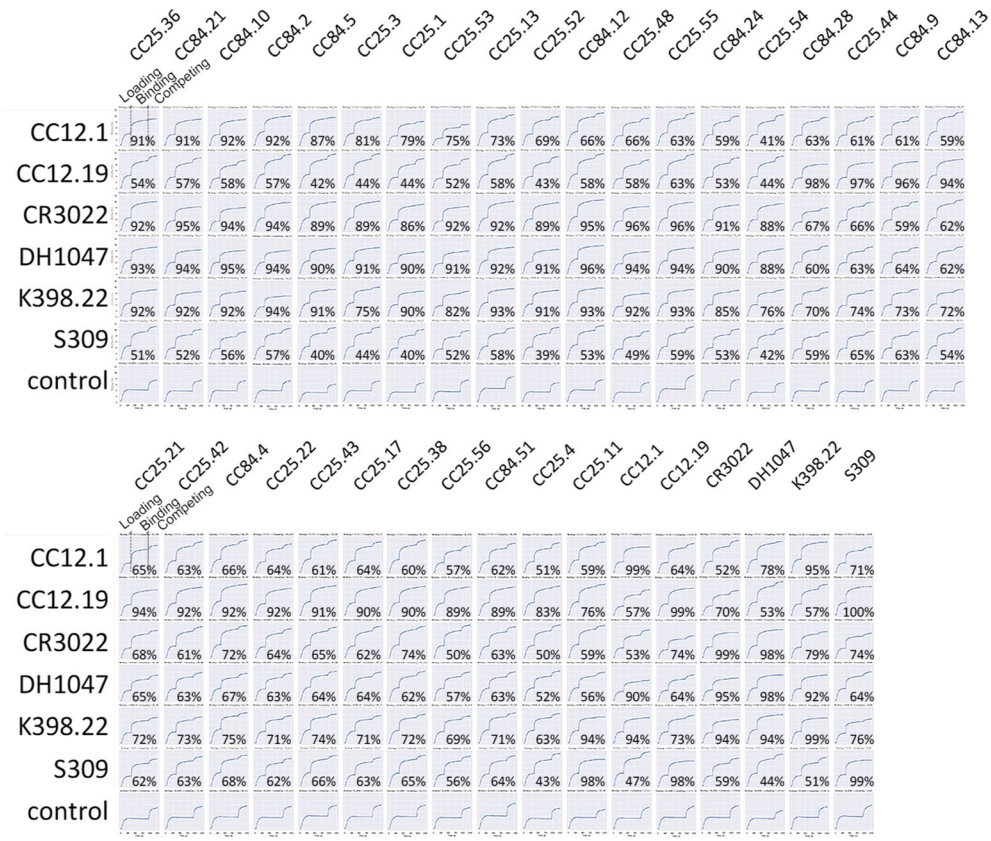

Extended Data Fig. 7 | Epitope binning of mAbs using a competition assay. 30 select mAbs (19 mAbs from donor CC25 and 11 mAbs from donor CC84) were assayed in BLI competition binning to evaluate epitope properties shared with previously isolated human (CC12.1, CC12.19, CR3022, DH1047 and S309) and macaque (K398.22) mAbs with known epitope specificities. His-tagged SARS-CoV-2 RBD protein (200 nM) was captured on anti-His biosensors and incubated with the indicated mAbs at a saturating concentration of 100 μg/mL for 10 mins and followed by nAb incubation for 5 min at a concentration of 25 μg/mL. All BLI measurements were performed on an Octet RED384 system. BLI traces are shown for each binding. The binding inhibition % is calculated with the formula: percent (%) of inhibition in the BLI binding response = 1- (response in presence of the competitor antibody / response of the corresponding control antibody without the competitor antibody).

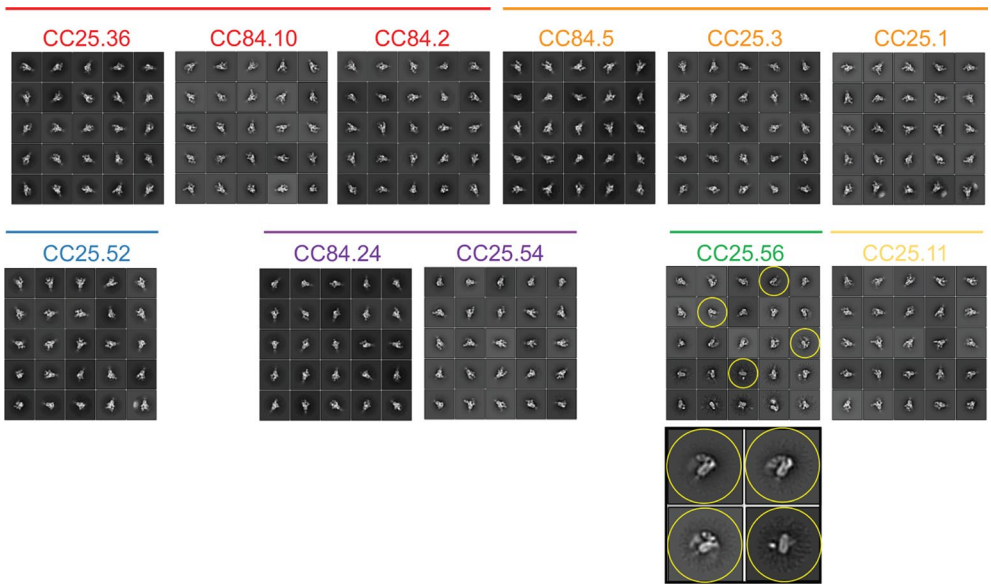

Extended Data Fig. 8 | Epitope mapping of bnAbs using negative stain Electron Microscopy (ns-EM). Electron microscopy (EM) images of sarbecovirus cross-neutralizing antibody Fabs with SARS-CoV-2 S-protein. 2D class averages of S-protein bound Fabs for each mAbs are shown. One of the group 2 bnAb Fabs, CC25.56, had some destabilizing effect on the S-protein trimer (indicated in yellow circles). The antibody S-protein complexing experiments were performed twice and consistent results were obtained.

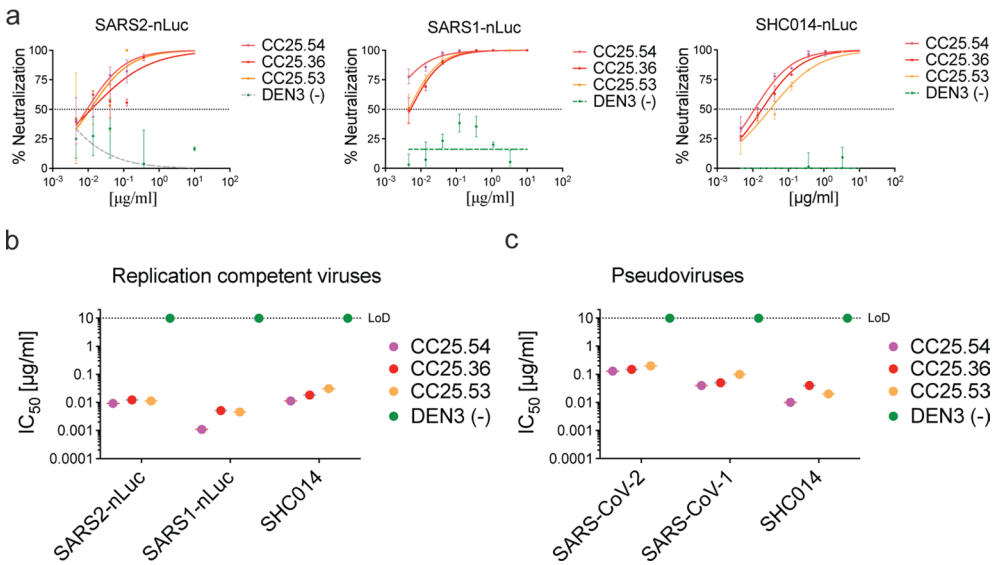

Extended Data Fig. 9 | Neutralization of replication competent sarbecoviruses by select RBD bnAbs. a. Neutralization of replication competent viruses encoding SARS-CoV-2 (SARS2-nLuc), SARS-CoV-1 (SARS1-nLuc) and SHC014 (SHC014-nLuc) by 3 select RBD bnAbs, CC25.54, CC25.36 and CC25.53. DEN3 antibody was a negative control for the neutralization assay. Data are presented as mean values +/- SD. **b-c**. Comparison of IC_{50} neutralization titers of 3 RBD bnAbs with replication-competent (**b**) and pseudoviruses (**c**) of SARS-CoV-2, SARS-CoV-1 and SHC014 ACE2-utilizing sarbecoviruses. Data are shown as scatter dot plots with line representing the mean. The experiments were independently performed twice and consistent results were obtained.

nature portfolio

Corresponding author(s): Ralph S. Baric, Lisa E. Gralinski, Dennis R. Burton, Raiees Andrabi

Last updated by author(s): April. 19, 2022

Reporting Summary

Nature Portfolio wishes to improve the reproducibility of the work that we publish. This form provides structure for consistency and transparency in reporting. For further information on Nature Portfolio policies, see our Editorial Policies and the Editorial Policy Checklist.

Statistics

For all statistical analyses, confirm that the following items are present in the figure legend, table legend, main text, or Methods section.

n/a	Confirmed
☐	☒ The exact sample size (*n*) for each experimental group/condition, given as a discrete number and unit of measurement
☐	☒ A statement on whether measurements were taken from distinct samples or whether the same sample was measured repeatedly
☐	☒ The statistical test(s) used AND whether they are one- or two-sided *Only common tests should be described solely by name; describe more complex techniques in the Methods section.*
☐	☒ A description of all covariates tested
☐	☒ A description of any assumptions or corrections, such as tests of normality and adjustment for multiple comparisons
☐	☒ A full description of the statistical parameters including central tendency (e.g. means) or other basic estimates (e.g. regression coefficient) AND variation (e.g. standard deviation) or associated estimates of uncertainty (e.g. confidence intervals)
☐	☒ For null hypothesis testing, the test statistic (e.g. *F*, *t*, *r*) with confidence intervals, effect sizes, degrees of freedom and *P* value noted *Give P values as exact values whenever suitable.*
☒	☐ For Bayesian analysis, information on the choice of priors and Markov chain Monte Carlo settings
☒	☐ For hierarchical and complex designs, identification of the appropriate level for tests and full reporting of outcomes
☒	☐ Estimates of effect sizes (e.g. Cohen's *d*, Pearson's *r*), indicating how they were calculated

Our web collection on statistics for biologists contains articles on many of the points above.

Software and code

Policy information about availability of computer code

Data collection	SoftMax Pro 5.4 Fortebio Data Acquisition 9.0 BD FACSChorus
Data analysis	GraphPad Prism 8 FlowJo v10.8.0 Fortebio Data Analysis version 12 IMGT V-Quest online tool version 3.5.29 Relion 3.0 UCSF Chimera DiversityAnalyzer tool ClusterW2 tool version 2.0 Iroki tool

For manuscripts utilizing custom algorithms or software that are central to the research but not yet described in published literature, software must be made available to editors and reviewers. We strongly encourage code deposition in a community repository (e.g. GitHub). See the Nature Portfolio guidelines for submitting code & software for further information.

Data

Policy information about availability of data

All manuscripts must include a data availability statement. This statement should provide the following information, where applicable:

- Accession codes, unique identifiers, or web links for publicly available datasets
- A description of any restrictions on data availability
- For clinical datasets or third party data, please ensure that the statement adheres to our policy

The authors declare that all the data supporting the findings of this study are available within the paper and its supplementary information files and any remaining information can be obtained from the corresponding author upon reasonable request. Antibody sequences have been deposited in GenBank under accession numbers OM467906 - OM468119. The negative stain electron microscopy (ns-EM) maps of RBD bnAb Fabs in complex with SARS-CoV-2 S-protein has been deposited to the Electron Microscopy Data Bank (EMDB) under accession IDs EMDB-26365-26375. Antibody plasmids are available from Raiees Andrabi or Dennis R. Burton under a standard material transfer agreement with The Scripps Research Institute.

Field-specific reporting

Please select the one below that is the best fit for your research. If you are not sure, read the appropriate sections before making your selection.

☒ Life sciences ☐ Behavioural & social sciences ☐ Ecological, evolutionary & environmental sciences

For a reference copy of the document with all sections, see nature.com/documents/nr-reporting-summary-flat.pdf

Life sciences study design

All studies must disclose on these points even when the disclosure is negative.

Sample size	The sample size was based on availability of the samples and patients.
Data exclusions	No data were excluded from the analyses.
Replication	For reproducibly, experimental assays were carried out in duplicates and repeated at least once for reproducibility, and all attempts at replication were successful.
Randomization	Randomization is not applicable in this study because the samples used for each experiments were grouped and data was obtained in the same batch in order to generate accurate comparison.
Blinding	The reported data in this study was based on quantitative measurements, including binding experiments and neutralization experiments etc. Therefore, blinding was not relevant given the fact that there is no subjective observations in this study.

Reporting for specific materials, systems and methods

We require information from authors about some types of materials, experimental systems and methods used in many studies. Here, indicate whether each material, system or method listed is relevant to your study. If you are not sure if a list item applies to your research, read the appropriate section before selecting a response.

Materials & experimental systems

n/a	Involved in the study
☐	☒ Antibodies
☐	☒ Eukaryotic cell lines
☒	☐ Palaeontology and archaeology
☒	☐ Animals and other organisms
☐	☒ Human research participants
☒	☐ Clinical data
☒	☐ Dual use research of concern

Methods

n/a	Involved in the study
☒	☐ ChIP-seq
☐	☒ Flow cytometry
☒	☐ MRI-based neuroimaging

Antibodies

Antibodies used	RAffiniPure goat anti-human IgG Fc fragment specific (Jackson ImmunoResearch Laboratories #109-055-008); anti-human CD3(APC Cy7, BD Pharmingen #557757), anti-human CD4(APC-Cy7, Biolegend #317418), anti-human CD8(APC-Cy7, BD Pharmingen #557760), anti-human CD19(PerCP-Cy5.5, Fisher Scientific #NC9963455), anti-human CD20 (PerCP-Cy5.5, Biolegend, #302326, clone 2H7), anti-human IgG(BV605, BD Pharmingen #563246) and IgM (PE, Biolegend, #314508, clone MHM-88), anti-human CD14(APC-Cy7, BD Pharmingen #561384, clone M5E2), mouse anti-His antibody (Invitrogen cat. #MA1-21315-1MG, ThermoFisher Scientific),

Streptavidin-AF488 (Thermo Fisher S32354), Streptavidin-BV421 (BD Biosciences 563259)

Validation

https://www.jacksonimmuno.com/catalog/products/109-055-008
https://www.thermofisher.com/antibody/product/6x-His-Tag-Antibody-clone-HIS-H8-Monoclonal/MA1-21315
https://www.bdbiosciences.com/us/reagents/research/antibodies-buffers/immunology-reagents/anti-non-human-primate-antibodies/cell-surface-antigens/apc-cy7-mouse-anti-human-cd3-sp34-2/p/557757
https://www.biolegend.com/en-us/products/apc-cyanine7-anti-human-cd4-antibody-3658?GroupID=GROUP28
https://www.bdbiosciences.com/us/reagents/research/antibodies-buffers/immunology-reagents/anti-non-human-primate-antibodies/cell-surface-antigens/apc-cy7-mouse-anti-human-cd8-rpa-t8/p/557760
https://www.bdbiosciences.com/us/applications/research/stem-cell-research/hematopoietic-stem-cell-markers/human/negative-markers/apc-h7-mouse-anti-human-cd14-m5e2/p/561384
https://www.biolegend.com/en-us/products/percp-cyanine5-5-anti-human-cd19-antibody-4226?GroupID=GROUP28
https://www.biolegend.com/en-us/products/percp-cyanine5-5-anti-human-cd20-antibody-4228
https://www.bdbiosciences.com/us/applications/research/b-cell-research/immunoglobulins/human/bv605-mouse-anti-human-igg-g18-145/p/563246
https://www.biolegend.com/en-us/products/pe-anti-human-igm-antibody-2878?GroupID=GROUP28
https://www.jacksonimmuno.com/catalog/products/109-035-006
https://www.thermofisher.com/antibody/product/MA1-21315-1MG.html?CID=AFLCA-MA1-21315-1MG
https://www.thermofisher.com/order/catalog/product/S11223
https://www.bdbiosciences.com/en-us/products/reagents/flow-cytometry-reagents/research-reagents/single-color-antibodies-ruo/bv421-streptavidin.563259

Eukaryotic cell lines

Policy information about cell lines

Cell line source(s)	HEK293F cell line was obtained from ThermoFisher; HEK293T cell line was obtained from ATCC; HeLa-ACE2 was made in house from the HeLa cell line obtained from ATCC. Expi293 cells were obtained from Life Technologies. Vero E6 cells were purchased from ATCC.
Authentication	No authentication was performed.
Mycoplasma contamination	The cell lines were not tested for mycoplasma.
Commonly misidentified lines (See ICLAC register)	No commonly misidentified cell lines were used.

Human research participants

Policy information about studies involving human research participants

Population characteristics	See Extended Data Fig. 10.
Recruitment	Plasma and PBMCs from convalescent COVID patients were provided through the "Collection of Biospecimens from Persons Under Investigation for 2019-Novel Coronavirus Infection to Understand Viral Shedding and Immune Response Study" UCSD IRB# 200236. COVID patient samples were collected based on COVID-19 diagnosis regardless of gender, race, ethnicity, disease severity, or other medical conditions. The age and the ethnicity variables were relatively evenly distributed across the human cohort.
Ethics oversight	Protocol was approved by the UCSD Human Research Protection Program.

Note that full information on the approval of the study protocol must also be provided in the manuscript.

Flow Cytometry

Plots

Confirm that:

☒ The axis labels state the marker and fluorochrome used (e.g. CD4-FITC).

☒ The axis scales are clearly visible. Include numbers along axes only for bottom left plot of group (a 'group' is an analysis of identical markers).

☒ All plots are contour plots with outliers or pseudocolor plots.

☒ A numerical value for number of cells or percentage (with statistics) is provided.

Methodology

Sample preparation	Frozen human PBMCs were re-suspended in 10 ml RPMI 1640 medium with 50% fetal bovine serum (FBS). After centrifugation at 400xg for 5 minutes, the cells were resuspended in a 5 ml FACS buffer (PBS, 2% FBS, 2mM EDTA). The cells were incubated with the mixture of fluorescently labeled antibodies to cell surface markers for 15 minutes on ice in the dark. The spike proteins of SARS-CoV-2 and SARS-CoV-1 were conjugated to fluorescently labeled streptavidin, and each spike-

	probe was added to the Ab-cell mixture and incubated for 30 minutes on ice in the dark. FVS510 Live/Dead stain in the FACS buffer (1:300) was added to the cells and incubated on ice in the dark for 15 minutes. The stained cells were washed with FACS buffer and re-suspended in 500 µl of FACS buffer/10-20 million cells, passed through a 70 µm mesh cap FACS tube and ready for sort.
Instrument	BD Melody sorter was used for flow cytometry data collection and single-cell sorting.
Software	FlowJo was used for flow cytometry analysis.
Cell population abundance	Purity checks on sorted cells were not performed due to limitation of post-sort cell number.
Gating strategy	After the gating of lymphocytes (SSC-A vs. FSC-A) and singlets (FSC-H vs. FSC-A), live cells were identified by the negative FVS510 Live/Dead staining phenotype, then antigen-specific memory B cells were distinguished with sequential gating and defined as CD3-, CD4-, CD8-, CD14-, CD19+, CD20+, IgM-and IgG+. Subsequently, spike-specific B cells were identified with the phenotype of AF488+BV421+AF647 (CoV2 S and CoV1 S double positive).

☒ Tick this box to confirm that a figure exemplifying the gating strategy is provided in the Supplementary Information.